EUREC4A

Bjorn Stevens, Sandrine Bony, David Farrell, Felix Ament, Alan M. Blyth, Chiristopher W. Fairall, Johannes Karstensen, Patricia K. Quinn, Sabrina Speich, Claudia Acquistapace, et al.

EUREC^{4}A

B. Stevens[1], S. Bony[2], D. Farrell[3], F. Ament[4,1], A. Blyth[5], C. Fairall[6], J. Karstensen[7], P. Quinn[8], S. Speich[9], F. Aemisegger[10], A. L. Albright[2], E. Bodenschatz[11], K.-A. Caesar[3], R. Chewitt-Lucas[3], J. Delanoë[12], G. De Boer[13,6], F. Ewald[14], M. Forde[3], G. George[1], A. Hausold[15], M. Hagen[14], L. Hirsch[1], F. Jansen[1], S. Kinne[1], D. Klocke[16], T. Kölling[17], H. Konow[4], W. Mohr[18], A. K. Naumann[1,19], L. Nuijens[20], R. Pincus[13,6], G. Reverdin[21], G. Roberts[22,23], S. Schnitt[24], P. Sullivan[25], L. Touzé-Peiffer[26], J. Vial[2], R. Vogel[2], C. Acquistapace[24], N. Alexander[3], L. Alves[27], S. Arixi[28], H. Asmath[29], G. Bagheri[11], A. Bailey[25], D. Baranowski[30], A. Baron[31], S. Barrau[28], P. A. Barrett[32], A. Behrendt[33], H. Bellenger[2], A. Bendinger[7], F. Beucher[34], S. Bigorre[35], P. Blossey[36], O. Bock[37], P. Bosser[38], D. Bourras[39], P. Bouruet-Aubertot[40], K. Bower[41], H. Branger[42], M. Brennek[43], A. Brewer[44], P.-E. Brilouet[45], B. Brügmann[1], S. A. Buehler[4], E. Burke[46], R. Burton[25], S. Böing[47], R. Calmer[13], J.-C. Canonici[48], X. Carton[49], G. J. Cato[50], J. A. Charles[51], P. Chazette[52], Y. Chen[53], T. Choularton[41], P. Chuang[54], S. Clarke[55], H. Coe[41], C. Cornet[56], P. Coutris[57], F. Couvreux[58], S. Crewell[24], T. Cronin[59], Z. Cui[47], Y. Cuypers[40], A. Daley[3], G. M. Damerell[60], T. Dauhut[1], D. De Graaf[l], G. De Groot[20], S. P. De Szoeke[61], L. Denby[47], H. Deneke[62], J.-P. Desbios[48], V. Douet[63], K. Drushka[64], M. Dütsch[65], A. Ehrlich[66], K. Emanuel[59], A. Emmanouilidis[66], J.-C. Etienne[34], S. Etienne-Leblanc[67], G. Faure[68], G. Feingold[44], L. Ferrero[69], B. Fildier[70], A. Fix[14], C. Flamant[71], P. J. Flatau[72], G. R. Foltz[73], L. Forster[17], A. Gadian[47], J. Galewsky[74], M. Gallagher[41], P. Gallimore[41], C. Gaston[75], C. Gentemann[76], N. Geyskens[77], A. Giez[15], C. Gourbeyre[57], S. Gross[14], R. Grosz[78], M. Gutleben[14], J. Güttler[11], K. Hall[3], G. Harris[79], K. C. Helfer[20], D. Henze[61], C. Herbert[79], K. J. Heywood[60], B. Holanda[80], A. Ibanez-Landeta[11], J. Intrieri[81], S. Iyer[64], M. Jacob[24], F. Julien[28], H. Kalesse[66], J. Kazil[13,44], A. Kellman[82], U. Kirchner[1], M. Klingebiel[1], L. A. Kremper[80], J. Kretzschmar[66], O. Krüger[80], A. Kurz[15], M. Körner[7], P. L'Hégaret[83], T. Lachlan-Cope[84], A. Laing[85], P. Landschützer[1], T. Lang[19,86], D. Lange[33], I. Lange[4], C. Laplace[87], R. Laxenaire[88], C. Le Bihan[89], M. Leandro[54], N. Lefevre[90], D. Lenschow[25], Q. Li[14], G. Lloyd[41], S. Los[91], N. Losi[92], M. Lothon[93], O. Lovell[94], C. Luneau[95], P. Makuch[96], S. Malinowski[97], G. Manta[9], E. Marinou[14,98], N. Marsden[41], L. Matthieu[99], N. Maury[34], B. Mayer[17], M. Mayers-Als[3], C. Mazel[100], W. McGeary[101,102], J. C. McWilliams[103], M. Mech[24], M. Mehlmann[7], A. N. Meroni[104], T. Mieslinger[4,86], A. Minikin[15], Y. Morfa Avalos[1], C. Muller[105], I. Musat[2], G. Möller[17], A. Napoli[104], A. Neuberger[1], D. Noone[106], F. Nordsiek[11], J. L. Nowak[43], L. Olivier[40], L. Oswald[14], D. J. Parker[47], C. Peck[107], R. Person[21], A. Plueddemann[35], L. Pologne[3], M. Posyniak[30], M. Prange[4], M. Pöhlker[80], C. Pöhlker[80], V. Pörtge[17], U. Pöschl[80], E. Quiñones Meléndez[108], J. Radtke[19,86], K. Ramage[63], J. Reimann[109], L. Renault[90], K. Reus[7], A. Reyes[3], J. Ribbe[110], M. Ringel[1], M. Ritschel[1], C. B. Rocha[35], N. Rochetin[9], C. Rollo[60], J. Röttenbacher[66], L. Saffin[47], S. Sandiford[3], I. Sandu[111], V. Schemann[24], I. Schirmacher[4], O. Schlenczek[11], J. Schmidt[112], M. Schröder[11], H. Schulz[1], A. Schwarzenboeck[57], M. Schäfer[66], A. Sealy[3], I. Serikov[1], S. Shohan[66], E. Siddle[60], A. P. Siebesma[20], F. Späth[33], C. C. Stephan[1], M. K. Stolla[1], W. Szkółka[30], S. Tarot[89], E. Tetoni[14], E. Thompson[6], J. Thomson[65], L. Tomassini[32], J. Totems[31], L. Villiger[10], A. Walther[113], B. Webber[60], M. Wendisch[66], S. Whitehall[3], A. Wiltshire[94], A. A. Wing[88], M. Wirth[14], J. Wiskandt[7], K. Wolf[66], L. Worbes[1], E. Wright[114], V. Wulfmeyer[33], S. Young[115], D. Zhang[116,8], C. Zhang[8], F. Ziemen[117], T. Zinner[17], P. Zuidema[118], M. Zöger[15]

[1]Max Planck Institute for Meteorology, Hamburg, Germany
[2]LMD/IPSL, Sorbonne Université, CNRS, Paris, France
[3]Caribbean Institute for Meteorology and Hydrology, Barbados
[4]Universität Hamburg, Hamburg, Germany
[5]National Centre for Atmospheric Science, University of Leeds, UK
[6]NOAA Physical Sciences Laboratory, Boulder, CO, USA
[7]GEOMAR Helmholtz Centre for Ocean Research, Kiel, Germany
[8]NOAA PMEL, Seattle, WA, USA
[9]LMD/IPSL, Ecole Normale Supérieure, Paris, France
[10]Institute for Atmospheric and Climate Science, ETH Zürich, Zürich, Switzerland
[11]Max Planck Institute for Dynamics and Self-Organization, Göttingen, Germany
[12]LATMOS/IPSL, Université Paris-Saclay, UVSQ, Guyancourt, France
[13]Cooperative Institute for Research In Environmental Sciences, University of Colorado, Boulder, CO, USA

[14]Deutsches Zentrum für Luft- und Raumfahrt, Institut für Physik der Atmosphäre, Oberpfaffenhofen, Germany
[15]Deutsches Zentrum für Luft- und Raumfahrt, Flugexperimente, Oberpfaffenhofen, Germany
[16]DWD Hans-Ertel-Zentrum für Wetterforschung, Offenbach, Germany
[17]Ludwig-Maximilians-Universitaet, Munich, Germany
[18]Max Planck Institute for Marine Microbiology, Bremen, Germany
[19]Institute of Meteorology, Center for Earth System Research and Sustainability, Universität Hamburg, Hamburg, Germany
[20]Delft University of Technology, Delft, The Netherlands
[21]LOCEAN/IPSL, Sorbonne Université, CNRS, Paris, France
[22]CNRM, Toulouse France
[23]Scripps Institution of Oceanography, University of California San Diego, La Jolla, CA, USA
[24]University of Cologne, Cologne, Germany
[25]National Center for Atmospheric Research, Boulder, CO, USA
[26]LMD/IPSL, Sorbonne Université, Paris, France
[27]Hydrometeorological Service, Guyana
[28]CNRM, Météo-France, CNRS, Toulouse, France
[29]Institute of Marine Affairs, Trinidad and Tobago
[30]Institute of Geophysics, Polish Academy of Sciences, Warsaw, Poland
[31]LSCE/IPSL, CEA, Gif-Sur-Yvette, France
[32]Met Office, Exeter, UK
[33]Institute of Physics and Meteorology, University of Hohenheim, Stuttgart, Germany
[34]CNRM, Météo-France, Toulouse, France
[35]Woods Hole Oceanographic Institution, Woods Hole, MA, USA
[36]Department of Atmospheric Sciences, University of Washington, Seattle, WA, USA
[37]IPGP, Paris, France
[38]ENSTA Bretagne, Lab-STICC, UMR, CNRS, Brest, France
[39]MIO, CNRS, Marseille, France
[40]LOCEAN/IPSL, Sorbonne Université, Paris, France
[41]University of Manchester, Manchester, UK
[42]Irphe, CNRS/Amu/Ecm, Marseille, France
[43]Institute of Geophysics, Faculty of Physics, University of Warsaw, Warsaw, Poland
[44]NOAA Chemical Sciences Laboratory, Boulder, CO, USA
[45]Laboratoire d'Aérologie, University of Toulouse, Toulouse, France
[46]St. Christopher Air & Sea Ports Authority, Basseterre, St. Kitts and Nevis
[47]University of Leeds, Leeds, UK
[48]Service Des Avions Français Instrumentés Pour La Recherche En Environnement, Cugnaux, France
[49]LOPS/IUEM, Université de Bretagne Occidentale, CNRS, Brest, France
[50]Argyle Meteorological Services, St. Vincent & The Grenadines
[51]Grenada Meteorological Services, Grenada
[52]LSCE/IPSL, CEA, Gif-sur-Yvette, France
[53]Ecole Normale Supérieure, Paris, France
[54]University of California Santa Cruz, Santa Cruz, CA, USA
[55]Cayman Islands National Weather Service, Cayman Islands
[56]LOA, Univ. Lille, CNRS, Lille, France
[57]LAMP, Université Clermont Auvergne, CNRS, Clermont-Ferrand, France
[58]CNRM, University of Toulouse, Meteo-France, Toulouse, France
[59]Massachusetts Institute of Technology, Cambridge, MA, USA
[60]University of East Anglia, Norwich, UK
[61]Oregon State University, Corvallis, OR, USA
[62]Leibniz Institute for Tropospheric Research, Leipzig, Germany
[63]IPSL, CNRS, Paris, France
[64]Applied Physics Laboratory, University of Washington, Seattle, WA, USA
[65]University of Washington, Seattle, WA, USA
[66]Leipzig Institute for Meteorology, University of Leipzig, Germany
[67]Meteorological Department St. Maarten
[68]Météo-France, Toulouse, France
[69]Gemma Center, University of Milano-Bicocca, Milan, Italy
[70]LMD/IPSL, École Normale Supérieure, Paris, France
[71]LATMOS/IPSL, Sorbonne Université, CNRS, Paris, France
[72]Scripps Institution of Oceanography, University of California San Diego, San Diego, CA, USA
[73]NOAA Atlantic Oceanographic and Meteorological Laboratory, Miami, FL, USA
[74]Department of Earth and Planetary Sciences, University of New Mexico, Albuquerque, NM USA
[75]University of Miami, Miami, FL, USA
[76]Farallon Institute, USA
[77]DT-INSU, CNRS, France
[78]Institute of Geophysics, University of Warsaw, Poland
[79]Regional Security Service, Barbados
[80]Max Planck Institute for Chemistry, Mainz, Germany
[81]NOAA Earth System Research Laboratory, Boulder, CO, USA
[82]Barbados Coast Guard, Barbados
[83]LOPS, Université de Bretagne Occidentale, Brest, France
[84]British Antarctic Survey, Cambridge, UK
[85]Caribbean Meteorological Organization, Trinidad and Tobago
[86]International Max Planck Research School On Earth System Modelling, Max Planck Institute for Meteorology, Hamburg, Germany
[87]IPSL, Paris, France
[88]Florida State University, Tallahassee, FL, USA
[89]Ifremer, Brest, France
[90]IRD, Brest, France
[91]University of New Mexico, Albuquerque, NM, USA
[92]Milano Bicocca University, Italy
[93]Laboratoire d'Aérologie, University of Toulouse, CNRS, Toulouse, France
[94]Trinidad and Tobago Meteorological Services, Trinidad and Tobago

[95]OSU Pytheas, Marseille, France
[96]The Institute of Oceanology of The Polish Academy of Sciences, Sopot, Poland
[97]University of Warsaw, Warsaw, Poland
[98]Institute for Astronomy, Astrophysics, Space Applications and Remote Sensing, National Observatory of Athens, Athens, Greece
[99]CNRS, France
[100]Dronexsolution, Toulouse, France
[101]Barbados Meteorological Services, Barbados
[102]Caribbean Institute For Meteorology And Hydrology, Barbados
[103]Department of Atmospheric and Oceanic Sciences, UCLA, Los Angeles, CA, USA
[104]CIMA Research Foundation, Savona, Italy
[105]LMD/IPSL, Ecole Normale Supérieure, CNRS, Paris, France
[106]University of Auckland, Auckland, NZ
[107]Meteorological Service, Kingston, Jamaica
[108]College of Earth, Ocean and Atmospheric Sciences, Oregon State University, Corvallis, OR, USA
[109]Deutsches Zentrum für Luft- und Raumfahrt, Institut für Hochfrequenztechnik und Radarsysteme, Oberpfaffenhofen, Germany
[110]University of Southern Queensland, Toowoomba, Australia
[111]European Centre for Medium Range Weather Forecasts, Reading, UK
[112]Naval Research Laboratory, Monterey, CA, USA
[113]University of Wisconsin-Madison, Madison, WI, USA
[114]Florida State University, Tallahassee, Florida, USA
[115]National Meteorological Service of Belize, Belize
[116]JISAO, University of Washington, Seattle, WA, USA
[117]Deutsches Klimarechenzentrum GmbH, Hamburg, Germany
[118]Rosenstiel School of Marine and Atmospheric Science/University of Miami, Miami, FL, USA

Corresponding author: Bjorn Stevens, `bjorn.stevens@mpimet.mpg.de`

Key Points:

- Description of EUREC^{4}A field campaign to test hypothesized cloud feedbacks and quantify factors influencing cloudiness in the trades.
- First measurements linking clouds to meso and sub-mesoscale motions in the lower atmosphere and upper ocean.
- Novel application of remote sensing and autonomous vehicles to study the remote marine environment.

Abstract
[enter your Abstract here]

Plain Language Summary

[enter your Plain Language Summary here or delete this section]

1 Introduction

Clouds are curious creatures. On the one hand they act as a metaphor for something fleeting, sensitive to subtle shifts in the wind, to the presence and nature of particulate matter, to small changes in radiant energy transfer, surface temperatures or myriad other factors (Siebesma et al., 2020). On the other hand, and from the view of the climate, their constancy is what is striking (Stevens & Schwartz, 2012). In terms of climate change, should even a little bit of their sensible side express itself with warming, large effects could result. This realization has motivated a great deal of research in recent years (Bony et al., 2015), research culminating in a recent field study, named EUREC^{4}A (*ElUcidating the RolE of Cloud-Circulation Coupling in ClimAte*). Its measurements, which this paper describes, represent the most ambitious effort ever to quantify how cloud-properties co-vary with their atmospheric and oceanic environment across a range of scales.

Initially EUREC^{4}A was proposed as a way to test hypothesized cloud-feedback mechanisms thought to explain large differences in model estimates of climate sensitivity, and to provide benchmark measurements for a new generation of models and satellite observations (Bony et al., 2017). To meet these objectives required quantifying different measures of clouds in the trades (trade winds) as a function of their large-scale environment. In the past, efforts to use measurements for this purpose – from BOMEX (Holland & Rasmusson, 1973) to ASTEX (Albrecht et al., 1995) to RICO (Rauber et al., 2007), see also Bannon (1949) – have been hampered by an inability to constrain the mean vertical motion over larger-scales, and by difficulties in quantifying something as multifaceted as a field of clouds (Bretherton et al., 1999; Stevens et al., 2001; Siebesma et al., 2003; vanZanten et al., 2011). EUREC^{4}A was made possible by emergence of new methods to measure these quantities, many of which were developed through experimentation over the past decade in and around the Barbados Cloud Observatory (Stevens et al., 2016; Stevens, Ament, et al., 2019). To execute these measurements required a high-flying aircraft (the German HALO operated by DLR) distributing a large number of dropsondes around the perimeter of a mesoscale (ca 200 km ⌀) circle to characterize the environment. A second low-flying aircraft (the French ATR-42 operated by SAFIRE), with in situ cloud sensors and sidewards staring active remote sensing, which complemented by nadir staring from the above flying aircraft, was necessary to determine the distribution of cloudiness and aspects of the environment difficult to characterize from the sondes. By making these measurements upwind of the Barbados Cloud Observatory, and adding a research vessel (the R/V Meteor) for additional surface based remote sensing and surface flux measurements, the environment and its clouds would be yet better constrained.

Quantifying day-to-day variations in both cloudiness and its environment, opened the door to additional questions, greatly expanding EUREC^{4}A's scope. In addition to testing hypothesized cloud feedback mechanisms, EUREC^{4}A's experimental plan was augmented to (i) quantify the relative role of micro and macrophysical factors in rain formation; (ii) quantify different factors influencing the mass, energy and momentum balances in the subcloud layer; (iii) identify processes influencing the evolution of ocean meso-scale eddies; (iv) measure the influence of ocean heterogeneity, i.e., fronts and eddies, on air-sea interaction and cloud formation; and (v) provide benchmark measurements for a new generation of both fine-scale coupled models and satellite retrievals. Complementing these scientific pursuits, EUREC^{4}A developed outreach and capacity building activities that allowed scientists coming from outside the Caribbean to benefit from local expertise and vice versa.

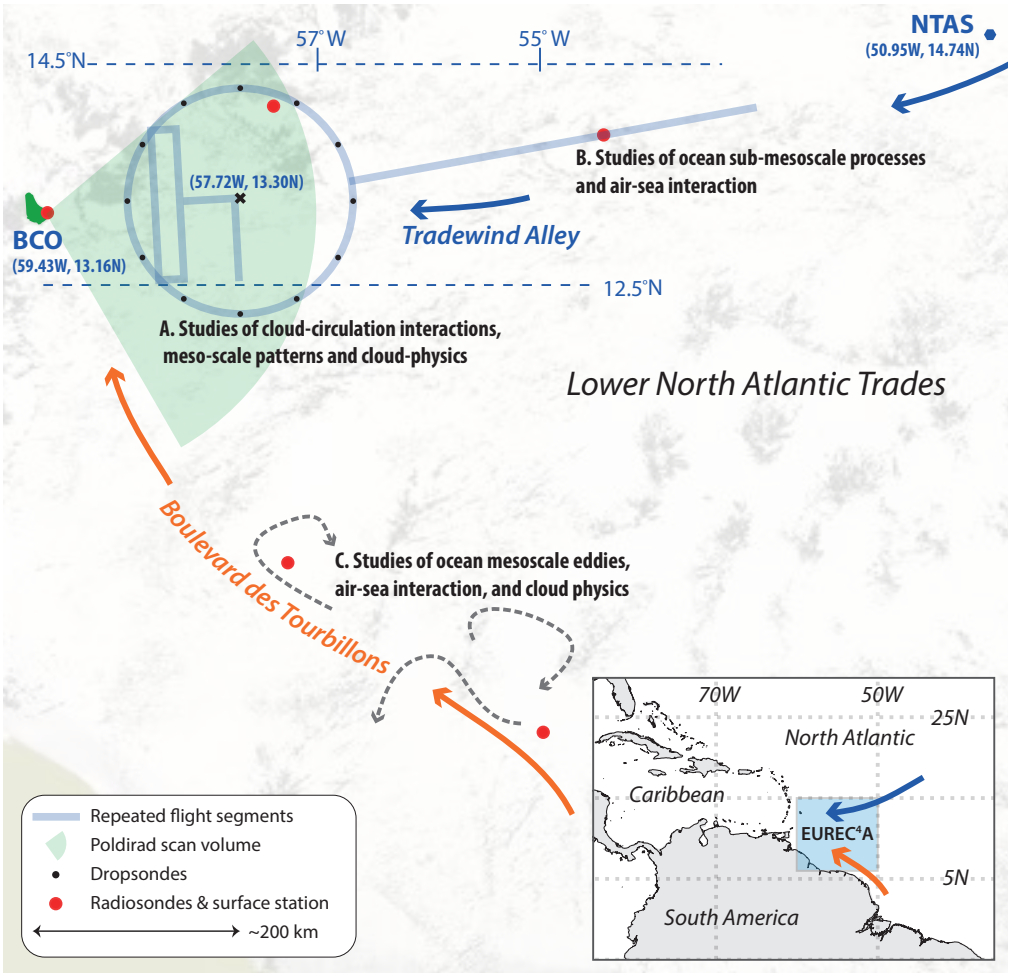

Figure 1. The EUREC^{4}A study area in the lower trades of the North Atlantic. The zonally oriented band following the directions of the trades between the Northwest Tropical Atlantic Station (NTAS) and the Barbados Cloud Observatory (BCO) is called Tradewind Alley. It encompasses two study areas (A and B). The EUREC^{4}A-Circle is defined by the circular airborne sounding array centered at 57.7°W. A third study area (C) followed the southeast to northwest meanders of what we called the Boulevard des Tourbillons. The background shows a negative of the cloud field taken from the 5 February, 2020 MODIS-Terra (ca 1430 UTC) overpass.

Addressing these additional questions required a substantial expansion of the activities initially planned by the Barbadian-French-German partnership that first proposed EUREC^{4}A. This was accomplished through a union of projects successfully proposed by additional teams of investigators. For instance, EUREC^{4}A-UK (a UK project), brought the British Antarctic Survey's Twin Otter (TO for short) and ground based facilities for aerosol measurements to advance cloud physics studies; EUREC^{4}A-OA secured the service of two additional research vessels (the French R/V L'Atalante and the German R/V Maria Sybilla Merian) and various autonomous observing platforms to study ocean process; and ATOMIC[1] brought an additional research vessel (the NOAA R/V Ronald H. Brown), assorted autonomous systems, and the NOAA WP-3D Orion, Ms Piggy, to help augment studies of air-sea and aerosol-cloud interactions. Further national initiatives funded a large-scale sounding array, the installation of a scanning precipitation radar, the deployment of ship-borne CloudKites, a network of water stable isotopologue measurements, as well as a rich assortment of uncrewed aerial and seagoing systems, among them fixed-wing aircraft, quad copters, drifters, buoys, gliders, and saildrones. Support within the region helped link activities to operational initiatives, such as a training programme for forecasters from the region, and fund scientific participation from around the Caribbean. The additional measurement platforms considerably increased the scope of EUREC^{4}A, whose operations were coordinated over a large (roughly 10°×10°, as shown in Fig. 1) within the lower trades near Barbados, making it possible to pursue the additional objectives outlined above and described in more depth below.

This article describes EUREC^{4}A in terms of seven different facets as outlined above. To give structure to such a vast undertaking we focus on EUREC^{4}A's novel aspects, but strive to describe these in a way that also informs and guides the use of EUREC^{4}A data by those who did not have the good fortune to share in its collection. The presentation (§3) of these seven facets is framed by an overview of the general setting of the campaign in § 2, and a discussion of more peripheral, but still important, aspects such as data access and the ecological impacts of our activities in § 4.

2 General setting and novel measurements

EUREC^{4}A deployed a wide diversity of measurement platforms over two theatres of action. These, the 'Tradewind Alley' and the 'Boulevard des Tourbillons', are illustrated schematically in Fig. 1. Tradewind Alley comprised an extended corridor with its downwind terminus defined by the BCO and extending upwind to the Northwest Tropical Atlantic Station (NTAS 51°W, 15°N), an advanced open ocean mooring installed and operated by the Woods Hole Oceanographic Institute since 2001. Measurements aimed at addressing the initial objectives of EUREC^{4}A were situated near the western end of the corridor, within the range of low-level scans of the C-band radar on Barbados. The area of overlap between the radar and the (∼200 km diameter) EUREC^{4}A-Circle (marked A in Fig. 1) defined a region of intensive measurements in support of studies of cloud-circulation interactions, cloud physics, and factors influencing the mesoscale patterning of clouds. Additional measurements between the NTAS and 55°W (Region B in Fig. 1) supported studies of air-sea interaction and provided complementary measurements of the upwind environment, including a characterization of its clouds and aerosols.

The Boulevard des Tourbillons describes the geographic region that hosted intensive measurements to study how air-sea interaction is influenced by mesoscale eddies, sub-mesoscale fronts, and filaments in the ocean (Region C in Fig. 1). Large (ca 300 km) warm eddies – which migrate Northwestward and often envelope Barbados, advecting large fresh-water filaments stripped from the shore of South America – created a laboratory well suited to this purpose. These eddies, known as North Brazil Current (NBC) Rings, form when the retroflecting NBC pinches off around 7°N. Characterizing these eddies further offered the possibility to expand the upper-air network of radiosondes, and to make contrasting cloud measurements in a potentially dif-

[1] Atlantic Tradewind Ocean–Atmosphere Mesoscale Interaction Campaign

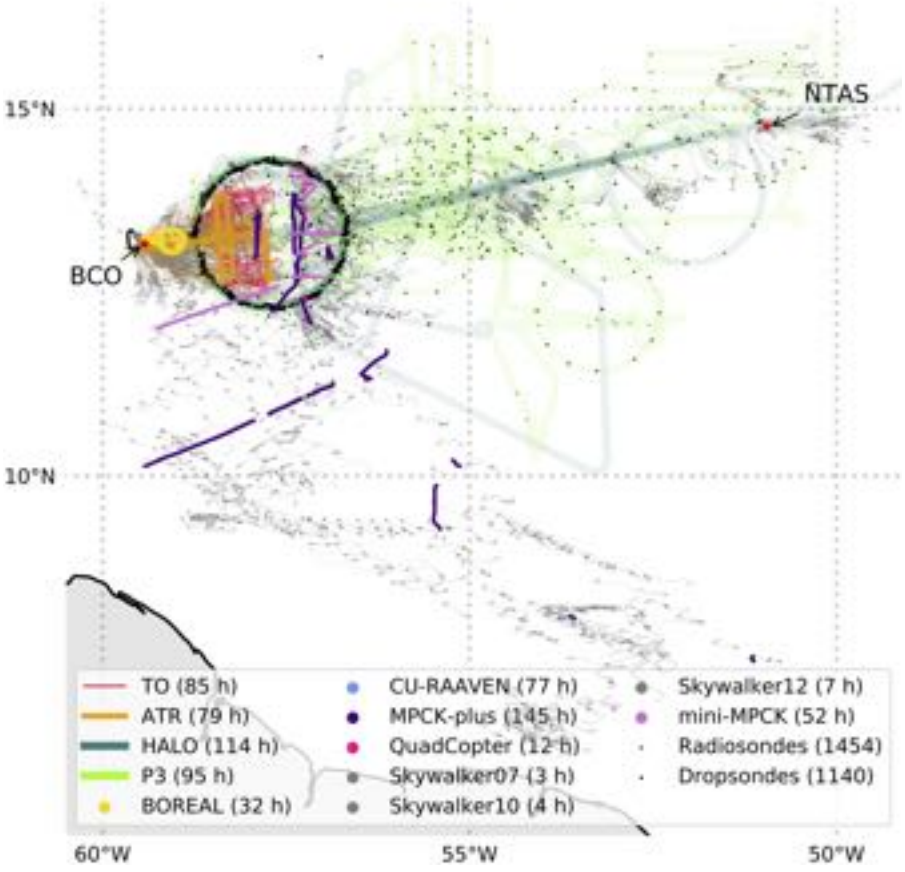

Figure 2. Domain of aerial measurements. Flight time for the crewed aircraft is for the period spent east of 59°W and west of 45°W. Radiosonde ascents and descents are counted separately but only when valid measurements are reported.

ferent large-scale environment. This situation led EUREC^{4}A to develop its measurements following the path of the NBC rings toward Barbados from their place of formation near the point of the NBC retroflection, with a center of action near Region C in Fig. 1.

2.1 Measurements of the lower atmosphere

Aerial measurements were made by research aircraft, uncrewed (i.e., remotely piloted) aerial systems (UASs), and from balloon or parachute borne soundings. These were mostly distributed along Tradewind Alley. Fig. 2 shows the realization of the original EUREC^{4}A strategy in the form of repeated Box-L flight pattern flown by the ATR (orange) within the EUREC^{4}A-Circle (mostly flown by HALO; teal, with black points for dropsondes). Excursions by HALO and flights by the P3 extended the area of measurements upwind of the EUREC^{4}A-Circle toward the NTAS. The TO intensively sampled clouds in the area of ATR operations in the western half of the EUREC^{4}A-Circle. UASs provided extensive measurements of the lower atmosphere, and because of their more limited range and need to avoid air-space conflicts with other platforms, concentrated in the area between the EUREC^{4}A-Circle and Barbados.

Different clusters of radiosonde soundings (evident as short grey lines) can also be discerned in Fig. 2. Those soundings originating from the BCO (342) in addition to those from the Meteor (362) were launched from relatively fixed positions, with the R/V Meteor operating between 12.5°N and 14.5°N along the 57.25°W meridian. East of the EUREC^{4}A-Circle, sondes were launched by the R/V Ronald H. Brown (Ron Brown), which mostly measured airmasses in coordination with the P3 measurements between the NTAS and the EUREC^{4}A-Circle. The R/V Maria Sybilla Merian (MS-Merian) and R/V L'Atalante (Atalante) combined to launch 424 sondes in total, mostly along the Boulevard. Except for the R/V Ron Brown, all platforms used radiosondes with parachutes, so that most launches resulted in two soundings, an ascent and a descent. The synoptic environment encountered during EUREC^{4}A and the radiosonde measurement strategy are described in detail by Stephan et al. (2020).

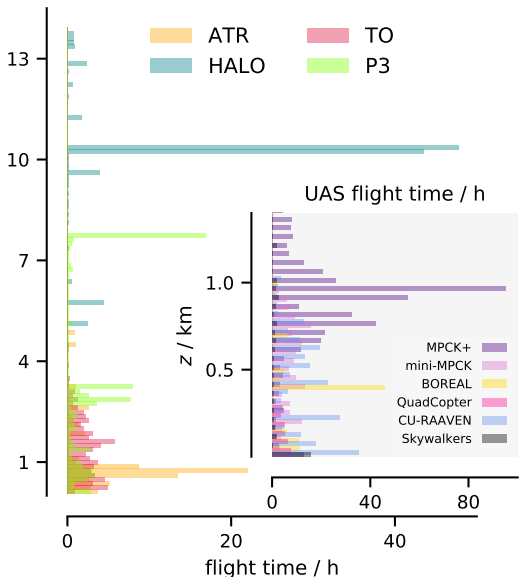

Figure 3. Sampling time at different altitudes by different airborne platforms

HALO, the ATR and most of the UASs emphasized statistical sampling. Hence flight plans did not target specific conditions, although the ATR flight levels were adjusted slightly

based on the estimated height of the boundary layer and cloud field that was encountered – but this varied relatively little. Measurements from the MPCK+ (a large CloudKite tethered to the R/V MS-Merian) emphasized the lower cloud layer selecting conditions when clouds seemed favorable. The mini-MPCK was used more for profiling the boundary layer and the cloud-base region, and was deployed when conditions (with regard to ship duty) allowed. The Twin Otter targeted cloud fields, often flying repeated samples through cloud clusters identified visibly. The P3 strategy was more mixed; some flights targeted specific conditions and others were more statistically oriented; for example, to fill gaps in the HALO and ATR sampling strategy. The different sampling strategies are reflected in Fig. 3 where the measurements of HALO are sharply concentrated at about 10.5 km and those of the ATR at about 800 m. Fig. 3 also shows the strong emphasis on sampling the lower atmosphere, with relatively uniform coverage of the lower 3 km. Except for the Twin-Otter, which was limited to daytime operations, take-off and landing times of the aircraft were staggered, with three night flights by the P3, to better sample the diurnal cycle. Data papers for the individual platforms are being prepared and will describe their activities in greater detail.

HALO performed several satellite underpasses as part of planned 'excursions' from its circling flight pattern. These included one underpass of MISR on 5 February 2020, and another under the core satellite of the Global Precipitation Mission (GPM) on 11 February, 2020.

2.2 Measurements of the upper ocean, and air-sea interface

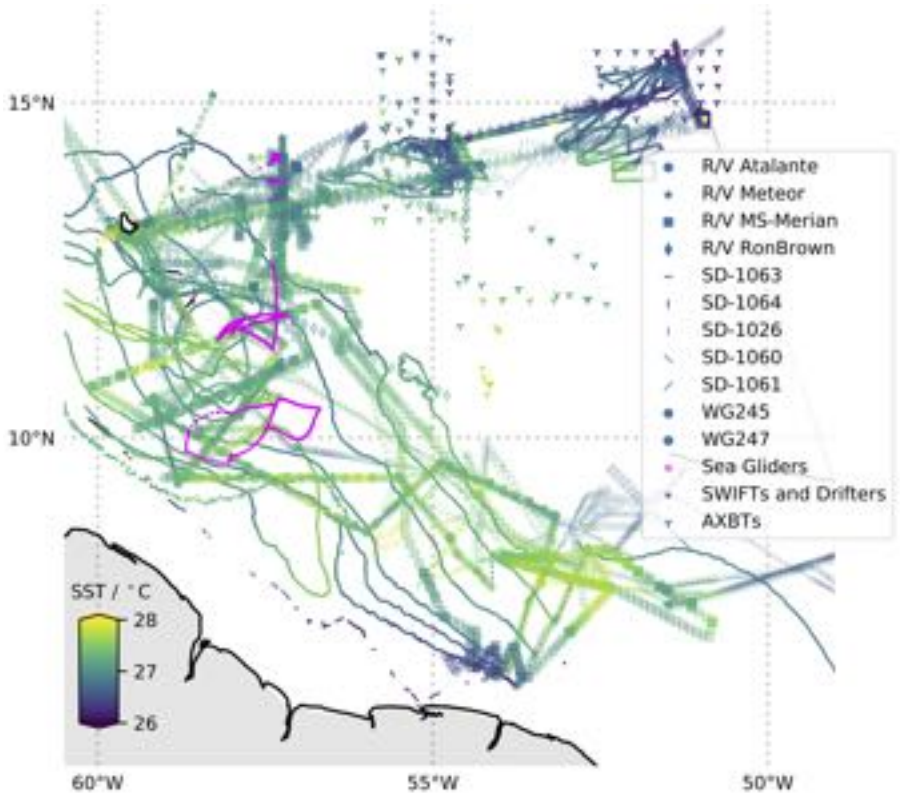

Figure 4. Map showing location of measurements by surface and sub-surface platforms

The oceanographic and air-sea interaction components of EUREC^{4}A were the main focus of the EUREC^{4}A-OA and ATOMIC projects, which supported the R/V Atalante, R/V MS-Merian and R/V Ron Brown measurements. In total, four research vessels – all equipped with surface meteorological measurements and underway temperature/salinity sampling devices –

and scores of autonomous surface and sub-surface vehicles were deployed along Tradewind Alley and the Boulevard des Tourbillons. The tracks of the surface vessels are shown in Fig. 4. These tracks, colored by measurements of the sea-surface temperature, show slightly more variability in water temperatures along the Boulevard des Tourbillons, in contrast with more steady westward warming of surface temperatures following the trades along Tradewind Alley. The more dynamic situation along the 'Boulevard', as compared to the situation on the 'Alley', required a different measurement strategy. For the former, research vessels actively tracked and surveyed mesoscale features, for the latter the sampling was more statistical so as to better support the airborne measurements and cloud characterization.

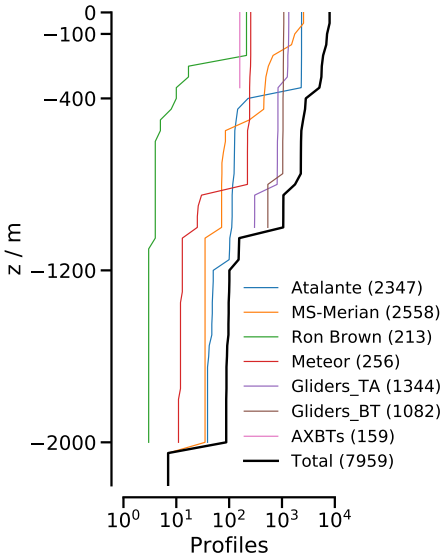

Figure 5. Number of profiles to sample a given depth. Ship based profiling is from CTD casts, underway CTDs, XBTs, and moving vessel profilers. AXBTs were dropped by the P3.

Along Tradewind Alley, the R/V Meteor mostly worked along the line of longitude at 57.25°W between 12.4°N and 14.2°N. The R/V Ron Brown, coordinating its measurements with the P3, was stationed between the NTAS and the Meridional Overturning Variability Experiment (50 nm northwest of the NTAS, not shown in Fig. 1) moorings in January, and in the region upwind of the EUREC^{4}A-Circle, near 55°W, in February. For both positions, SWIFT buoys were deployed and recovered in coordination with P3 Airborne Expendable Bathythermograph (AXBT) soundings. A Saildrone, two wave gliders, an AutoNaut (Caravela), four sea-gliders, and extensive Conductivity-Temperature-Depth (CTD) casts from the two ships profiled the upper ocean Fig. 5.

Along the Boulevard des Tourbillons the R/V MS-Merian and the R/V Atalante studied the meso- and submesocale dynamics. Both research vessels extensively profiled the ocean's upper km using a wide assortment of instruments, including underway CTDs, Moving Vessel Profilers, vertical microstructure profilers (VMP and MSS), Expendable Bathythermographs (XBTs) and Expendable CTDs (XCTDs). Three ocean gliders (one French SeaExplorer, two Slocum electric glider) provided dense sampling (more than 1300 profiles, most to at least 700 m, Fig. 5) of subsurface structures associated with mesoscale eddies. Of the roughly eight thousand upper ocean profiles performed during EUREC^{4}A, nearly three fourths were performed in coordination with the eddy sampling along the 'Boulevard'. Four Saildrones, 22 drifters and four deployments of two air-sea fluxes observing prototypes, OCARINA and PICCOLO substantially expanded the observations at the ocean-atmosphere interface. Five Argo floats equipped

with a dissolved oxygen sensor were deployed to allow a Lagrangian monitoring of the ocean surface and subsurface dynamics during and after the campaign.

To effectively survey features in the active waters of the Boulevard des Tourbillons the sampling strategy and cruise plan were assessed daily, using information from the past day's measurements, updates from satellite products, weather forecasts, and ocean predictions. Tailored satellite products and model predictions were provided by a variety of groups[2] to help track and follow surface features in near real time.

2.3 Novel measurement clusters

EUREC^{4}A set itself apart from past field studies both through new types of measurements, as performed by individual platforms, but also through the quantity or clustering of certain types of measurements. These clusters gave rise to a different quality of measurement as compared to what has been done in the past, especially in marine environments. Examples are described below and include the use of remote sensing, instruments for measuring stable water isotopologues, and drones,

2.3.1 Remote Sensing

EUREC^{4}A included eight (W or Ka band) high-sensitivity Doppler cloud radars. Four zenith staring instruments were installed at surface sites (BCO, R/V MS-Merian, R/V Meteor, and R/V Ron Brown) and three on aircraft (nadir, zenith on the ATR, HALO and the P3). The ATR flew a second, horizontally staring, Doppler system. Two scanning radars (a C-band system installed on Barbados, and a P3 X-band tail radar), and three profiling rain radars (one at the BCO, another at the Caribbean Institute for Meteorology and Hydrology and a third on the R/V Meteor), measured precipitation. The R/V MS-Merian additionally had an X-Band radar installed for wave characteristics and surface currents over a roughly 2 km footprint around the ship. Fourteen lidars were operated, four of which were advanced (high-spectral resolution, multi-wavelength) Raman or DIAL systems for profiling water vapor and aerosol/cloud properties. The Raman systems (at the BCO, on the R/V MS-Merian and R/V Meteor) were upward staring surface mounted systems, the DIAL operated in a downward looking model from HALO. On the ATR a backscatter UV lidar operated alongside the horizontally staring radar, looking horizontally to provide an innovative plan-form view of cloudiness near cloud base. Six wind-lidars and three ceilometers were operated from the BCO and all Research Vessels except for the R/V Atalante. As an example of the synergy the combination of these sensors provides, Fig. 6 shows ship based profiling of water vapor fluxes estimate from co-located wind-lidar and water vapor lidar measurements aboard the R/V MS-Merian.

More standard, but still unprecedented by virtue of its space-time-frequency coverage, was the contribution of airborne, surface and space-based passive remote sensing to EUREC^{4}A. Three 14-channel microwave radiometers operated from surface platforms, and a 25 channel downward staring system operating from HALO. Handheld sun-photometer measurements were made on all four research vessels and an automated system operated from Ragged Point, near the BCO, provided additional constraints on estimates of aerosol loading (from lidars) and column water vapor (from radiometers). Infrared radiometers for measuring the surface skin temperature were operated on the ATR, HALO, the R/V Ron Brown, the BOREAL and CU-RAAVEN UAVs, and on the five Saildrones. For estimating fluxes of radiant energy, broadband longwave and shortwave radiometers were installed on three of the airborne (zenith and nadir) and surface (zenith) platforms. In addition, HALO and the R/V Meteor hosted high-spectral resolution systems measuring shortwave and near-infrared down-welling radiances. From satellites near-real-time geostationary GOES-East satellite imagery and cloud product retrievals be-

[2] Collecte Localisation Satellite, the Centre Aval de Traitement des Données, Mercator Ocean, and the Center for Ocean-Atmospheric Prediction Studies

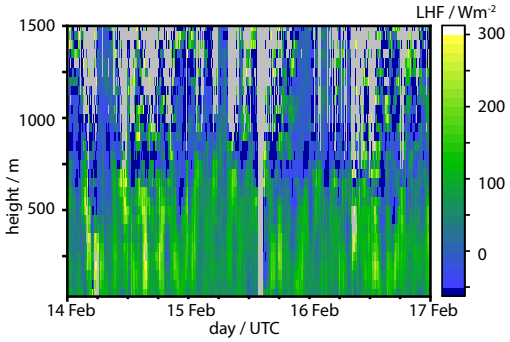

Figure 6. Synergy showing ship-based remotely sensed latent heat flux from the combination of Raman water vapor lidar and wind lidar aboard the R/V MS-Merian. The mean value over the three day period is 100 W m^{-2} at 200 m.

tween 19°N-5°S, 49°W-66°W were collected, with finer temporal resolution of every minute (between 14 January and 14 February, with a few data gaps due to the need to support hazardous weather forecasting in other domains) archived over most of this domain. ASTER's high-resolution (15 m visible and near infrared, and 90 m thermal) imager on board of TERRA was activated between 7°N-17°N and 41°W-61°N. It recorded 412 images of 60 km × 60 km in 25 overpasses between 11 January and 15 February. These images are complemented by Sentinel-2 data with images at 10 m resolution in some visible-near-infrared bands and 20 m resolution in shortwave-infrared bands relevant for cloud microphysical retrievals.

The intensity of remote sensing instrumentation in the vicinity of the EUREC^{4}A-Circle should support efforts to, for the first time, observationally close the column energy budget over the ocean.

2.3.2 Stable water isotopologues

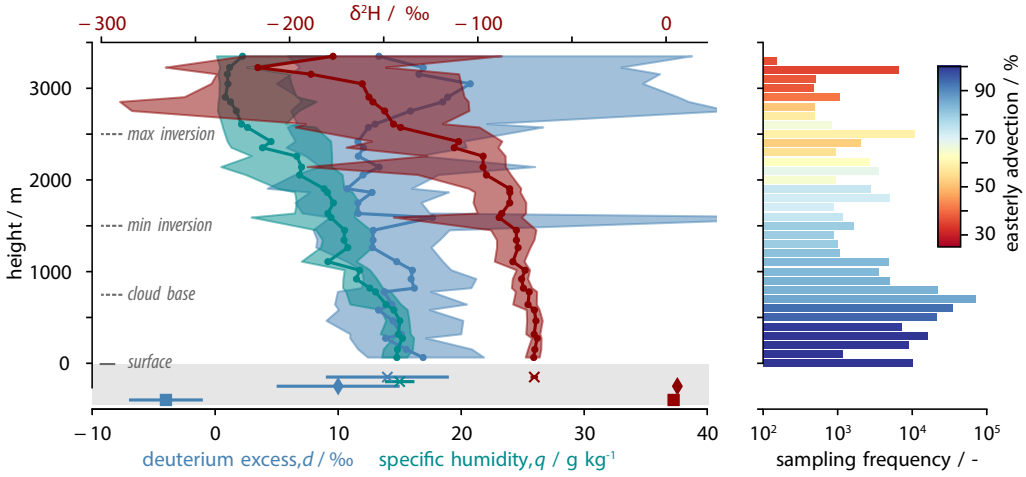

Figure 7. Water stable-isotopologues measurements during EUREC^{4}A

EUREC^{4}A benefited from an unusually complete and spatially extensive network of stable water isotopologue measurements ($H_2^{18}O$, $H_2^{16}O$, and HDO) distributed across multiple plat-

forms. Seven laser spectrometers and five precipitation sampling systems especially designed to avoid post-sampling re-evaporation were deployed. At the BCO, two laser spectrometers provided robust high-frequency measurements of isotopologues in water vapour and 46 event-based precipitation samples were collected. Three ships – the R/V Atalante, the R/V Meteor, and the R/V Ron Brown – were similarly equipped, and in addition collected ocean water samples (340 in total) from the underway water line and the CTDs. These samples have been analysed in the laboratory together with fifty ship-board rainfall samples. Two of the high-frequency laser spectrometers were mounted on the ATR and P3 to measure the vertical distribution of water isotopologues. The airborne measurements also added continuity, sampling air-masses between the BCO and R/V Meteor stations and between the R/V Meteor and the upwind R/V Ron Brown. The measurements provided very good coverage through the depth of the lower (3 km) atmosphere. Lagrangian and air-parcel backward trajectories based on wind fields from the operational ECMWF analyses indicate that boundary layer air came almost exclusively from the East, with a more isotropic origin of air-masses sampled above 2500 m (Fig. 7). Large-scale context for the in-situ measurements will be provided by retrievals of atmospheric HDO and $H_2^{16}O$ from space-borne instruments.

The size of the network of isotopologue measurements and the degree of coordination among the different measurement sites will enable investigations of the variability of the stable water isotopologues – in space and time, in ocean water, atmospheric vapor, and precipitation following the trades – that were previously not possible.

2.3.3 Drones and tethered platforms

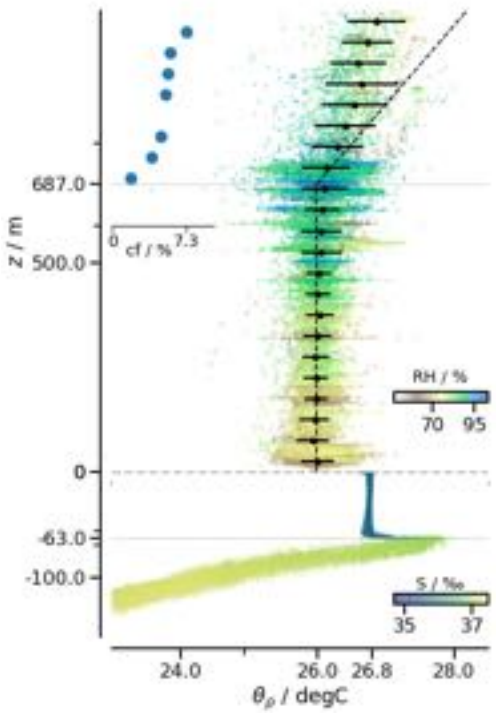

Figure 8. Typical ocean and atmospheric boundary layer upwind of the BCO. The black dashed line show the isentropic lapse rate of moist air with the measured near surface properties; the slope discontinuity at the lifting condensation level marks the shift from an unsaturated to a saturated isentrope.

A diversity of tethered and remotely piloted platforms provided measurements in the lower atmosphere and upper ocean. Many of these had been used in past field studies, but what set EUREC^{4}A apart was its coordinated use of so many platforms. Five fixed wing systems and a quad-copter provided approximately 200 h of open ocean atmospheric profiling, while seven sea-gliders profiled the underlying ocean porpoising well over a thousand times, mostly between the surface and 700 m. Fig. 8 presents measurements from one of the sea-gliders, and the CU-RAAVEN which along with the other fixed-wing systems (Boreal and Skywalkers) was flown from Morgan Lewis, a windward beach about 20 km north of the BCO. The measurements highlight the boundary-layers on either side of the air-sea interface, one (in the atmosphere) extending to about 700 m, and capped by a layer that is stably stratified with respect to unsaturated, but unstable with respect to saturated convection. The typical ocean mixed layer was as impressively well mixed, but over a layer about ten times shallower. Here the measurements document the peculiar situation of salinity maintaining the stratification that caps the downward growth of the ocean mixed layer. Ship-based measurements of the air-sea interface were greatly extended by five sail-drones, three wave-gliders, six Swift buoys, two autonomous prototype drifters (OCARINA and PICCOLO), and twenty-two drifters. In Fig. 8 the air-sea temperature difference of about 0.8 K is based on sail-drone data, which also quantifies the role of moisture in driving density differences. During EUREC^{4}A more than half of the density difference between the near-surface air, and air saturated at the skin-temperature of the underlying ocean, can be attributed to variations in the specific humidity.

Kite stabilized helium balloons, known as Max Planck Cloud Kites (MPCKs, or CloudKites) made their campaign debut during EUREC^{4}A. Three systems were flown, one large one (the MPCK+, with a lift of 115 kg) and a ceiling of near 1.5 km sampled clouds from the R/V MS-Merian. Two smaller CloudKites, one also flown from the R/V MS-Merian and the other from the R/V Meteor, had less lift and a slightly lower ceiling They focused on boundary layer and cloud-base profiling. Measurements from the CloudKites are used to quantify the cloud coverage in Fig. 8.

3 EUREC^{4}A's Seven Science Facets

In this section we elaborate on scientific (and social) topics that motivated EUREC^{4}A and how the measurements were specifically performed to address them. The presentation aims to emphasize advances as compared to had been possible in the past, yet not loose sight of the need to also provide a clear sketch of the campaign as a whole. Additional details describing the activities of specific platforms, or groups of platforms, are being described in complementary data papers, and a full listing of the instrumentation deployed is presented in appendices.

3.1 Testing hypothesized cloud-feedback mechanisms

As described by Bony et al. (2017), EUREC^{4}A was conceived as a way to test the hypothesis that enhanced mixing of the lower troposphere desiccates clouds at their base, in ways that warming would enhance (Rieck et al., 2012; Sherwood et al., 2014; Brient et al., 2016; Vial et al., 2016), but the signal of which has not been possible to identify in past measurements (Nuijens et al., 2014). In addition, recent research suggests that clouds in the trades tend to organize in mesoscale patterns (Stevens, Bony, et al., 2019) selected by environmental conditions (Bony et al., 2020). These findings raise the additional question as to whether changes in the mesoscale cloud organization with evolving environmental conditions might play a role in low-cloud feedbacks. To address these questions, EUREC^{4}A developed techniques to measure the strength of convective-scale and large-scale vertical motions in the lower troposphere, to estimate the cloud fraction near cloud-base, and to quantify possible drivers of changes in mesoscale cloud patterns, such as coherent structures within the subcloud layer, radiative cooling or air-mass trajectories, as well as their subsequent influence on cloud properties.

To make the desired measurements required HALO and the ATR to fly closely coordinated flight patterns, ideally sampling different phases of the diurnal cycle. This was realized

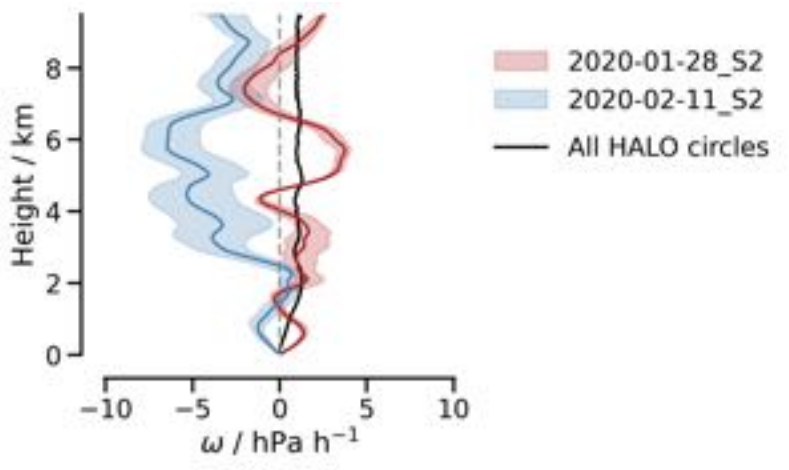

Figure 9. Dropsonde based estimates of vertical motion

by HALO circling at 10.5 km, three and a half times, over 210 min. Within this period three full sounding circles were defined by a set of twelve dropsonde launches, one for each 30° change in heading. The start time of successive sounding circles was offset by fifteen minutes so as to distribute the sondes through the period of circling. During this time HALO also provided continuous active and passive remote sensing of the cloud field below. Flying 50 min 'box' patterns just above the estimated cloud base (usually near a height of about 800 m, Fig. 3), the ATR provided additional remote sensing, as well as in-situ turbulence and cloud microphysical measurements. After two-to-three box patterns, the ATR flew two-to-four 'L'-shaped wind-aligned and wind-perpendicular patterns (the 'L' in Fig. 1) at the top, middle and bottom of the sub-cloud layer, before returning to Barbados to refuel for a second mission. While the ATR was refueling, HALO made an excursion, usually in the direction of the R/V Ron Brown and the NTAS buoy. On all but two occasions the ATR returned to the measurement zone after refueling (about 90 min later) to execute a second round of sampling, accompanied by HALO returning for another 210 min tour of the EUREC^{4}A-Circle. All told this resulted in eighteen coordinated (4 h flight segments), one of which involved the P3 substituting for HALO on one of its night-time flights.

A first target of the flight strategy was the measurement, for each sounding circle, of the vertical profile of mass divergence using dropsondes following Bony & Stevens (2019). In Fig. 9 the vertical pressure velocity, ω, estimated from this divergence is averaged over a set of three circles for two different days, and presented along with the average over all circles over all days. The figure shows how much the measured vertical velocity varied from flight to flight, with peak magnitudes many times the campaign mean. It also shows, for the first time from measurements on this scale, how the mean ω reduces to the expected climatological profile, with a magnitude (of about 1 hPa h^{-1}) similar to what is expected if subsidence warming is to balance radiative cooling.

The second target of the flight strategy was the measurement of the cloud fraction at cloud base through horizontal lidar-radar measurements by the ATR. In fields of optically-thin shallow cumuli (such as those associated with "Sugar" cloud patterns on January 28), cloud droplets were too small to be detected by the radar but the lidar could detect the presence of many successive clouds along a roughly 10 km line of sight (i.e. half of its box-pattern width, Fig. 10). In the presence of larger cloud droplets, normally associated with larger or more water laden clouds, such as on February 11, the radar detected larger droplets and rain drops over a range of 10 km (Fig. 10). The lidar-radar synergy will provide, for each rectangle, the cloud fraction and the distribution of cloud geometric and optical properties at cloud base. The second,

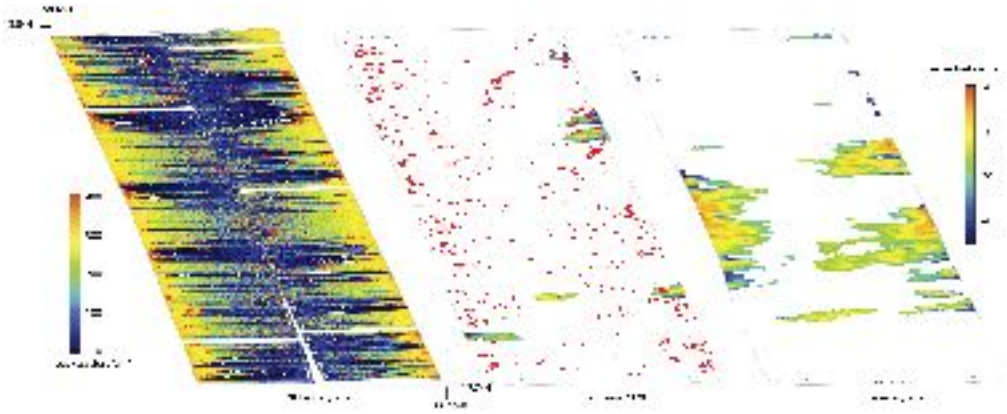

Figure 10. Illustration, for January 28, February 5, and February 11, of the cloud field observed at cloud base by the ATR with horizontal lidar and radar measurements. The left panel (28 Jan) shows only lidar data (attenuated backscatter signal corrected for molecular transmission), the right panel (11 Feb) shows only radar-reflectivity data and the middle panel (5 Feb) shows radar reflectivity and lidar cloud mask.

vertically pointing ATR cloud radar, allows a characterization of the aspect ratio of clouds, which may help infer the mesoscale circulations within the cloud field. These measurements, associated with new methods developed to estimate the cloud-base mass flux (Vogel et al., 2020), and to characterize the mesoscale cloud patterns from GOES-16, MODIS or ASTER satellite observations (Stevens, Bony, et al., 2019; Mieslinger et al., 2019; Bony et al., 2020; Denby, 2020; Rasp et al., 2020), will make it possible to test cloud feedback mechanisms and advance understanding as to whether mesoscale cloud patterns influence the hypothesized feedback mechanisms.

3.2 Quantifying processes influencing warm rain formation

As highlighted by Bodenschatz et al. (2010), the range of scales, from micro to mega meters, that clouds encompass has long been one of their fascinating aspects. EUREC^{4}A sought to quantify, for the first time, the main processes that influence trade-wind clouds across this full range of scales. By doing so it sought to answer long-standing questions in cloud physics, including: (i) whether whether microphysical processes substantially influence the net amount of rain that forms in warm clouds, and (ii) how important is the interplay between warm-rain development and the mesoscale organization of cloud fields. These questions identify precipitation development as the key process that links processes across scales, and hence guided EUREC^{4}A's measurement strategy.

On the particle scale, measurements targeted characterizing aerosols, within, upwind (by the R/V Ron Brown) within (from aircraft), and downwind (BCO and Ragged Point observatories), as well as more generically quantifying the effect of turbulence on droplet clustering (using Holographic imaging from the MPCK+), and turbulent mixing (from in situ sampling by the Twin Otter). All of these are thought to influence the formation of precipitation (Cooper et al., 2013; Broadwell & Breidenthal, 1982; Li et al., 2018; Wyszogrodzki et al., 2013), sometimes in opposing ways. For example, by acting as an additional source of CCN, dust may retard the formation of precipitation (Levin et al., 1996; Gibson et al., 2007; Bailey et al., 2013), but if present as giant CCN, it may have the opposite effect (Jensen & Nugent, 2017).

On the cloud scale, the intensity of rain and the evaporation of raindrops can lead to downdrafts, cold pools and mesoscale circulations which can lift air parcels, producing secondary and more sustained convection (e.g., Snodgrass et al., 2009). These cloud-scale circulations, which were a focus of measurements along and within the EUREC^{4}A-Circle, may also change

the vigor and mixing characteristics of cloud. This could in turn influence precipitation formation, a process that Seifert & Heus (2013) suggest may be self reinforcing, consistent with an apparent link between precipitation and mesoscale cloud patterns such as 'Fish' or 'Flowers' (Stevens, Bony, et al., 2019).

On larger (20 km to 200 km) scales, horizontal transport which determines whether or not Saharan dust reaches the clouds, as well as factors such as the tropospheric stability, or patterns of mesoscale convergence and divergence, which influences cloud vertical development, may affect the efficiency of warm rain production. In addition to the characterization of the environment from the dropsondes, the positioning of surface measurements (R/V Meteor, R/V Ron Brown, and BCO) helped characterize the Lagrangian evolution of the flow, also in terms of aerosol and cloud properties.

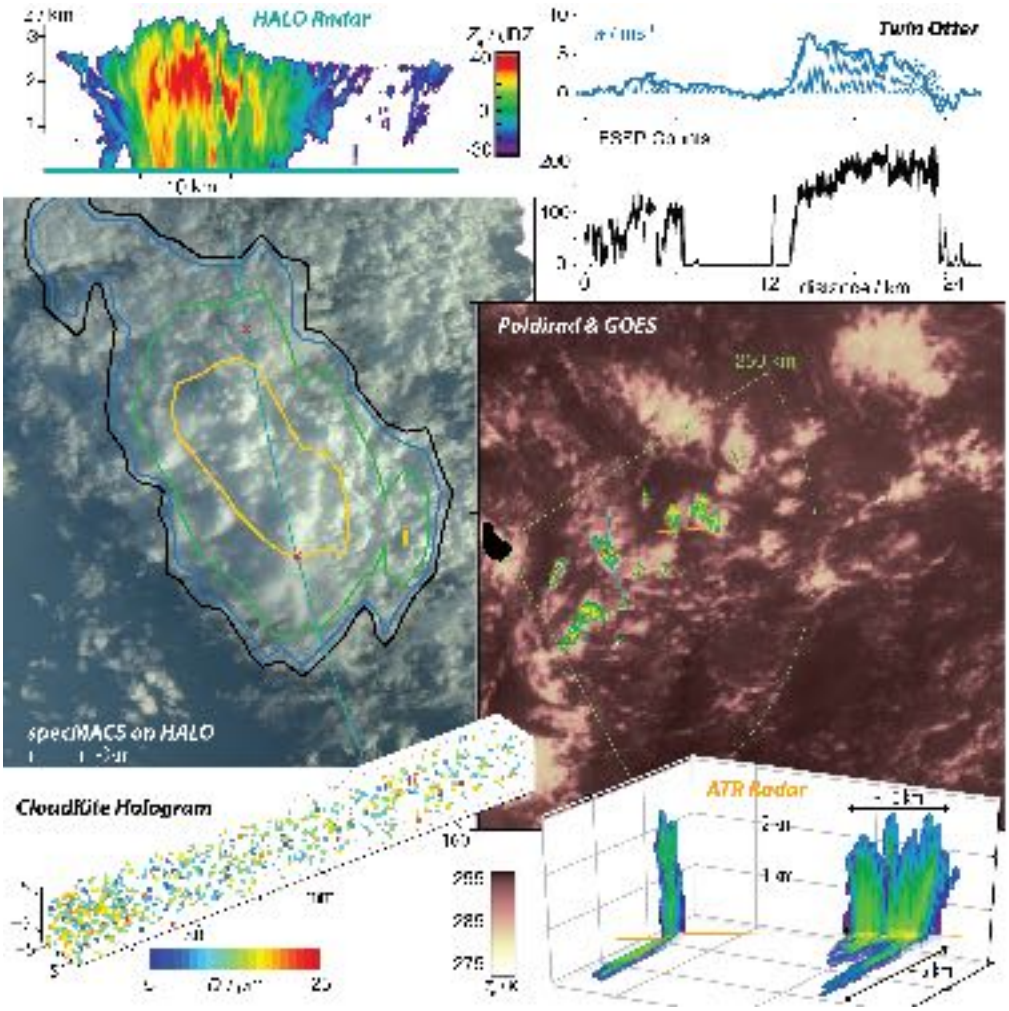

Figure 11. Composition of scales from different cloud sensing instrumentation, highlighting the test-section of the Tradewind Alley Cloud Chamber. POLDIRAD scans are overlain on satellite imagery from GOES with segments of the Twin-Otter, HALO and ATR flight tracks. Radar images from the ATR (horizontal and zenith) and HALO (nadir) are shown as well as a penetration of cloud from the Twin-Otter. specMACS image (missing) shows HALO cloud visualization along flight track. Hologram measurements from the MPCK+ were made in the southern portion of the circle (12.25°N, 57.70°W) at 1084 m on 17 February.

Fig 11 shows an example of the cascade of measurements, spanning scales covering ten orders of magnitude. On the smallest O(10^{-5} m) scale, a sample holographic image from an instrument mounted on the MPCK+ shows the spatial and size distribution of individual cloud drops. In-situ measurements and airborne remote sensing document the cloud microphysical structure and its relationship to the properties of the turbulent wind field. On scales of hundred meters to a few kilometers, vertically and horizontally cloud radars and lidars characterize the geometry and the macrophysical properties of clouds. On yet larger O(10^5 m) scales, the spatial organization and clustering of clouds and precipitation features is captured by satellite, by high-resolution radiometry from high-altitude aircraft, and by the C-band scanning radar, POLDIRAD.

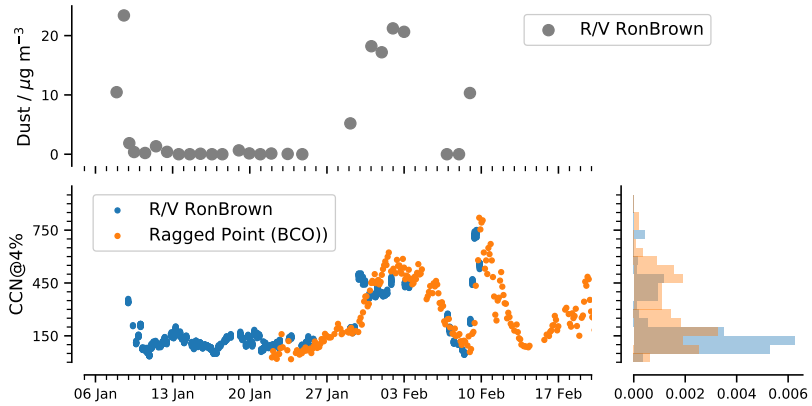

Figure 12. Aerosol characteristics in the Tradewind Alley over the period of measurements. Dust mass density from the R/V Ron Brown (upper left), which was mostly east of 55°W.Cloud condensation nuclei population densities that activate at a super-saturation of less than 0.4 % as measured from the Ragged Point Mast (400 m across a cove from the BCO) and from the R/V Ron Brown (lower left), normalized histogram of CCN from the time-series data (lower right).

An example of how the measurements upwind and downwind of the EUREC^{4}A-Circle helped constrain its aerosol environment is shown in Fig 12. Two periods of elevated CCN population densities (near 450 cm^{-3}), both associated with periods of elevated mineral dust, can be identified in measurements made aboard the R/V Ron Brown (East of 55°W) and from the ground station at Ragged Point (near the BCO). The slight lag of the Ragged Point measurements relative to those on the R/V Ron Brown is consistent with the positioning of the two stations and the westward dust transport by the mean flow. The episodes of elevated dust are believed to be from Saharan dust outbreaks, which are unusual in the (Boreal) winter months (Prospero, 1999). In between these events, CCN population densities are threefold smaller (150 cm^{-3}), which we take as representative of the clean maritime environment. Capturing such large perturbations in varying cloud conditions should aid efforts to untangle the relative role of different factors influencing warm-rain formation.

3.3 Subcloud mass, matter, energy and momentum budgets

Early field studies extensively and compellingly documented the basic structure of the lower atmosphere in the trades (Riehl et al., 1951; Malkus, 1958; Augstein et al., 1974; Brummer et al., 1974; Garstang & Betts, 1974). What remains poorly understood is the relative role of specific processes, particularly those acting at the mesoscale, in influencing this structure. A specific question that EUREC^{4}A aims to answer is the importance of downdrafts, and associated cold pools (Rauber et al., 2007; Zuidema et al., 2012), in influencing boundary layer thermodynamics structure and momentum transport to the surface. A related question is whether

the links between the cloud and sub-cloud layer depends on the patterns of convective organization, for instance as a result of differences in the circulation systems that may accompany such patterns.

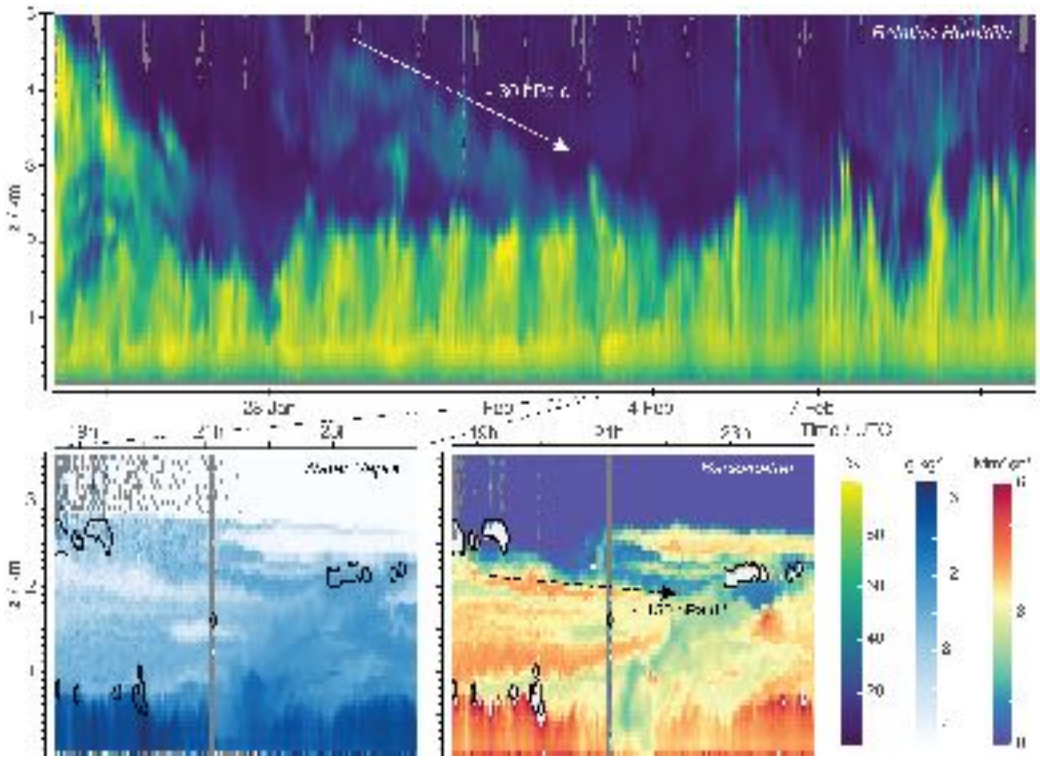

Figure 13. Lidar profiling of the lower atmosphere using the CORAL lidar at the BCO. Upper panel shows the relative humidity in the lower 5 km over the entirety of the campaign. Lower panels show the specific humidity over a four hour period marked by a large intrusion of cloud layer air on 2 February, and the associated aerosol/cloud backscatter. Also shown are the Lagrangian evolution of humidity, or backscatter features, as indicative of the magnitude of vertical velocity variations on different temporal scales.

For quantifying the subcloud layer budgets, as for many other questions, a limiting factor has been an inability to measure mesoscale variability in the vertical motion field. EUREC^{4}A's measurements not only address this past short coming, but the addition of the ship-based sounding network quantifies the multi-scale evolution of this important quantity. The arrangement of measurements, particularly flight segments, additionally helps quantify the Lagrangian evolution of air-masses in ways that help address some of these questions. In this respect, flight-legs were repeated on every mission at levels specifically attuned to the known structure of the lower-troposphere i.e., near the surface, in the middle, near the top and just above the sub-cloud layer, as well as in and just above the cloud layer. Past studies using a single aircraft, albeit in a more homogeneous environment, demonstrate that such a strategy can close boundary layer moisture and energy budgets (Stevens et al., 2003). Doing so allows a quantification of the vertical profile of turbulent transport and contributions associated with horizontal heterogeneity. It also sets the stage for estimating mass and energy budgets through the entire atmospheric column.

To address the measurement challenge posed by an environment rich in mesoscale variability, EUREC^{4}A made use of additional aircraft and a larger array of surface measurements (also from uncrewed platforms) as well as extensive ship and airborne active remote sensing, and a network of water stable-isotopologues (as presented in 2.3.2). At the BCO, aboard the

R/V Meteor and on the R/V MS-Merian, advanced Raman lidars provided continuous profiling of water vapor, clouds, temperature and aerosols. The nadir staring WALES lidar on HALO likewise profiled water vapor, clouds and aerosols. As an example of this capability, Fig. 13 presents relative humidity data (deduced from temperature and absolute humidity retrievals) from the BCO lidar. These measurements document the time-height evolution of water vapor in the boundary layer, something impossible to assess from airborne measurements, which measure at only a few levels, or soundings, which are sparse in time.

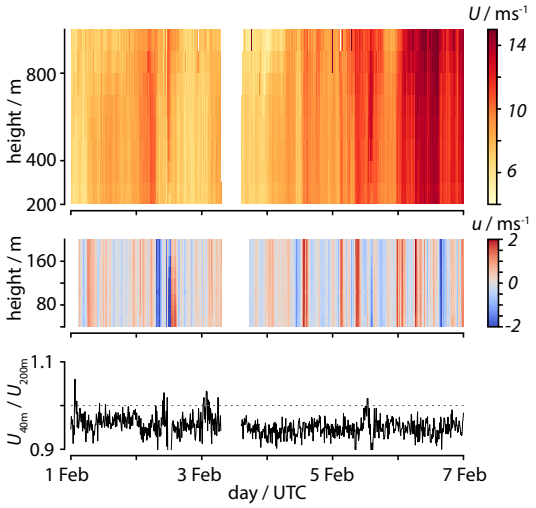

Figure 14. Wind lidar profiling of sub-cloud layer winds from the R/V Meteor. The upper panel shows the value of the zonal wind in the sub-cloud layer, above 200 m. Fluctuations of the near surface zonal wind from a three-hourly running mean value are shown in the zoom in the middle panel. Lower time-series shows the ratio of the 40 m wind (relevant for wind turbines and surface fluxes) from its value at 200 m.

The BCO lidar measurements quantify the structure of moist or dry layers in the free atmosphere, as well as variations in the cloud and subcloud layers, illustrating days of more nocturnal activity (centered on Feb 1), and also features presumed to be the signature of mesoscale circulations. The latter is the focus of the zoom in the lower panels which shows the lower 3 km over five hour period late on February 2, 2020. It shows a period where aerosol-poor air appears to descend adiabatically into the cloud layer (near 2 km, coincident with a large-scale fold of cloud-layer air into the subcloud layer. This results in a sharp contact discontinuity (aerosol front) near 21 UTC, which extends to the surface and is also evident in the water-vapor field. Typically the marine boundary (subcloud) layer is viewed as a turbulent layer that primarily interacts with the much larger-scale evolution of the free atmosphere through small scale entrainment at its top. Events such as the one shown in Fig. 13, suggest that in addition to downdrafts and the cold pools they feed, circulations on scales commensurate with and larger than the depth of the subcloud layer may be important for boundary layer budgets.

Similar considerations also apply to the momentum budget of the trades. Idealized large-eddy simulations by Dixit et al. (2020) under-estimate the flux of momentum to the surface, something they hypothesize to arise from an absence of meoscale circulations in the simulations. As an example of efforts to quantify such processes Fig. 14 shows the total wind speed measured in the sub-cloud layer by the long-range wind lidar aboard the R/V Meteor. The lower panel documents kilometer-scale wind speed variations on the order of 2 m s^{-1} that extend into the surface layer (derived from the short-range wind lidar, defined with respect to three-hourly running means). One question asked is whether at a given surface friction, convectively driven flows can sustain a relatively large near-surface wind, and weaker surface layer wind shear,

than expected from shear-driven turbulence alone. The third panel shows that the ratio of 40 m to 200 m wind speeds, as a measure of surface layer wind shear, is regularly close to 1. Combined with surface heat and momentum fluxes measured by other platforms, the lidars provide a unique opportunity to identify the influence of (moist) convection on wind stress at the surface.

3.4 Ocean mesoscale eddies and sub-mesoscale fronts and filaments

Mesoscale eddies, fronts, and filaments – not unlike the mesoscale circulations that are the subject of increasing attention in the atmosphere – are coherent structures that may be important for linking surface mixed layer to the interior ocean dynamics (Carton, 2010; Mahadevan, 2016; McWilliams, 2016). By virtue of a sharp contrast with their surroundings, these structures can efficiently transport enthalpy, salt, and carbon through the ocean. Though satellite observations have enhanced knowledge of their occurrence and surface imprint, the sparsity of direct observations limits our ability to test our understanding of such structures, in particular subsurface eddies. Understanding of the role of these types of structures is further limited by their short lifespans (hours to days) and small spatial scales (0.1 km to 10 km), which make them difficult to observe. These facts motivated ocean observations during EUREC^{4}A, as did recent work suggesting that such coherent structures, in particular localized upwelling, downwelling, straining, stratification variability, wave breaking, and vertical mixing, may couple with and influence atmsopheric processes, including cloud formation (Lambaerts et al., 2013; Renault et al., 2016; Foussard et al., 2019).

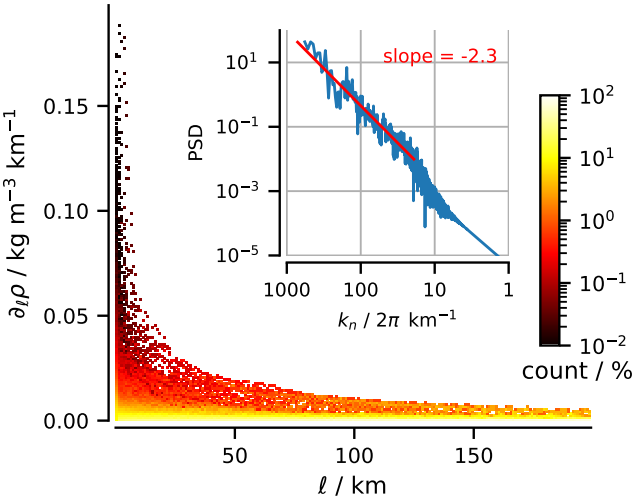

Figure 15. Percentage count of surface density gradients at different horizontal length scales (1 km to 200 km) measured by Saildrones; note the log scale colorbar. Inset is power spectral density of the surface density gradients, calculated by averaging Periodograms constructed for each vehicle after detrending the data and smoothing the data with a 2 km Gaussian filter. The red line shows the linear regression best fit slope of -2.3.

To address these questions, measurements during EUREC^{4}A attempted to quantify how near-surface currents, density, and waves varied across and within different dynamical regimes, e.g., for mesoscale eddies, fronts, and filaments. Such measurements aimed to answer specific questions not unlike those posed for the atmospheric boundary layer, namely to quantify the contribution of such structures to the spatial and temp oral variability of the upper ocean. EUREC^{4}A distinguished itself from past campaigns that have attempted similar measurements – LatMix: (Shcherbina et al., 2013); OSMOSIS: (Buckingham et al., 2016); CARTHE: (D'Asaro et al.,

2018) – by virtue of the number and diversity of observing platforms deployed (Saildrones, underwater gliders, instrumentally enhanced surface and subsurface drifters, wave gliders, an Autonaut, and biogeochemical Argo floats). These mapped the ocean down to 1000 m or more, simultaneously across both the Tradewind Alley and the Boulevard des Tourbillons (Fig. 2). These measurements have resulted in an unprecedented view of a large spectrum of ocean temporal and spatial scales across different oceanic environments.

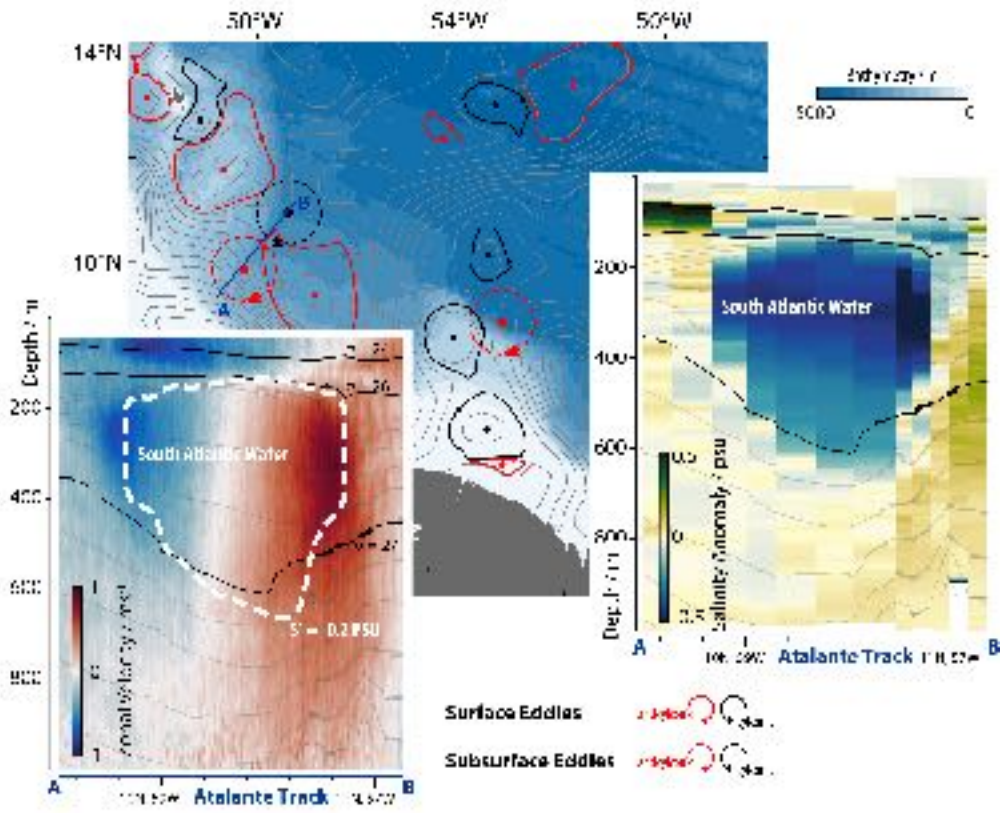

Figure 16. Measurement of a subsurface freshwater eddy near 58°W 10°N. Background map presents Absolute Dynamic Topography from Ssalto/Duacs. This shows the remotely sensed surface eddy field (Pujol et al., 2016), with features moving toward the northwest through the Boulevard des Tourbillons, and to the West along Tradewind alley. Eddy contours as detected automatically by the TOEddies algorithm (Laxenaire et al., 2018). The position of subsurface eddies (200 m to 600 m deep) as identified from the eddy detection method (Nencioli et al., 2010) applied to vector currents measured by Ship Acoustic Doppler Current Profilers (SADCP) are shown by circles. Overlain vertical transects show the zonal velocity component from the two SADCPs of the RV Atalante, and the salinity from CTD soundings as measured across one of the sections (A-B) that sampled surface and subsurface eddies evolving in the region. The surface and subsurface eddies appear to be evolving independently. The subsurface eddy freshwater anomaly is indicative of South Atlantic origins.

The richness of structure observed in the upper ocean during EUREC^{4}A can be quantified by the distribution of surface temperature fronts. All seagoing platforms contributed to observing the upper-ocean temperature structure, surveying a wide region and a large spectrum of ocean scales, and thus can contribute to this measure of upper ocean variability. An

example from one such platform, a Saildrone, is shown in Fig. 15. The sensitivity of frontal density gradients to spatial resolution was explored by subsampling data from 0.08 km to 100 km (Fig. 15. For each length scale, the percentage frequency of each density gradient was calculated. This analysis demonstrates that smaller length scales yield larger density gradients. The largest gradients were found at spatial scales of only 1 km and were associated with strong, local freshening. These are believed to be associated with small-scale, but intense, rain showers, an interesting finding given the importance of rain for linking processes at different scales in the atmosphere (e.g., §3.2). The analysis further documents self-similar (powerlaw) scaling between 19 km and 1900 km with a slope of -2.3. There is evidence of a scale break at around 25 km. Surface quasi-geostrophic turbulence generally predicts a slope of -5/3 or steeper (Callies & Ferrari, 2013; Rocha et al., 2016; Lapeyre, 2017).

A wide array of instruments deployed from all four ships (CTDs, underway CTDs, Mounted Vessel Profilers, microstructure profilers, XBTs, XCTDs, doppler current meter profilers, 5 BGC Argo floats) and the seven ocean gliders (e.g., Fig. 5) profiled water properties and ocean currents. This array of measurements, guided by near-real time satellite data and real-time ship profiling, revealed a surprisingly dense and diverse distribution of mesoscale eddies. All of the measured eddies captured by satellite data (Fig. 16) were shallow, extending to a depth of about 150 m (Fig. 16) and transporting warm and salty North Atlantic tropical water swiftly northward. Below but not aligned with the surface structures and separated by strong stratification, large subsurface anticyclonic eddies (and on some occasions cyclonic eddies) extended from 150 m to 800 m and carried large quantities of water from the South Atlantic northward. An example sampled by R/V Atalante along a Southwest to Northeast aligned transect near 50°N and 58°W is illustrated in Fig. 16. Here a ca 200 km eddy characterized by a 0.2 PSU freshwater anomaly was measured carrying water, which likely subducted in the south Atlantic, northward. The anomaly was associated with a circulation of $\approx 1\,\mathrm{m\,s^{-1}}$ with maximum velocities near 300 m extending downward to a depth of about 800 m. EUREC^{4}A observations such as these will be essential for understanding the complex dynamics of the upper ocean, and the extent to which they can be captured by a new generation of km scale coupled climate models.

3.5 Air-sea interaction

What distinguished EUREC^{4}A from the many previous campaigns focused on air-sea interaction was its interest in assessing how circulation systems, in both the ocean and the atmosphere, influence surface exchange processes. These interests extended to interactions with ocean biology and their impact on both CO_2 exchange and profligate amounts of sea-grass (Sargassum) that have, in past years, developed into a regional hazard. To study these processes EUREC^{4}A made use of a flotilla of uncrewed devices, and a wealth of nadir staring airborne remote sensing, specifically designed to characterize the air-sea interface on a range of scales.

Ocean eddies, fronts and filaments, influence the atmosphere by perturbing air-sea surface fluxes (Chelton & Xie, 2010; O'Neill et al., 2012) a process that may also feedback on the ocean (Renault et al., 2018). As an example, Sullivan et al. (2020) use large-eddy simulation to show how small scale ocean fronts perturb the boundary layer through its depth, giving rise to circulations on scales much larger than that of the boundary layer, or of the front itself (their Fig. 12). These lead to large perturbations in vertical mixing and, one can speculate, on patterns of cloudiness. Similarly, clouds influence the downward longwave and shortwave irradiance, which influences both the sea-surface temperature, but also atmospheric temperatures directly, something that Naumann et al. (2019) have shown to commensurately power (2 km to 200 km) circulations.

In the area of intensive measurements near and within the EUREC^{4}A-Circle (Region A), measurements sought to quantify how surface exchange proesses vary with circulation (cloud pattern) regime. Measurements by Caravela (a wave glider) and three sea-gliders characterized the air-sea interface in a small, and spatially fixed, (ca 10 km) region in this domain (Fig. 17).

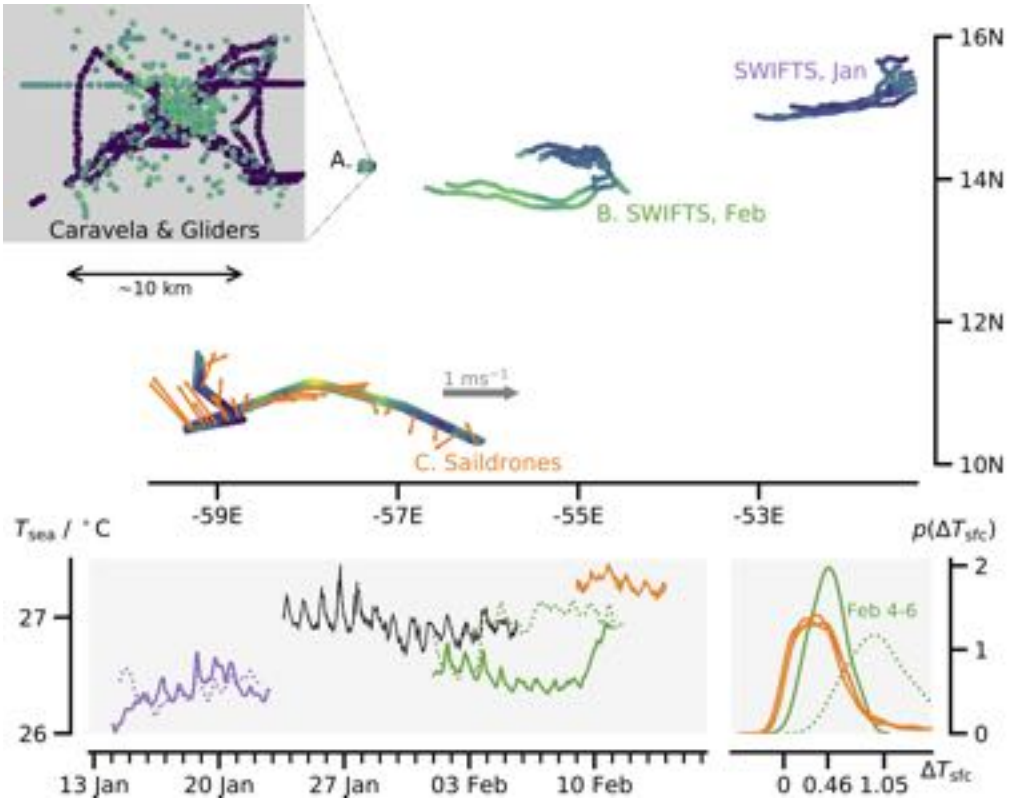

Figure 17. Uncrewed vehicles were used to study different aspects of air-sea interaction in all three of the EUREC^{4}A study regions. Upper panel shows the tracks of the instruments colored by their measurements of near surface water temperature,T_{sea}. The zoom (upper left0 expands the regional domain of the Caravela (and sea-glider) measurements in Region A (near 57°W. SWIFT buoys (T_{sea} at -0.3 m) were deployed on two ocassions in Region B. Saildrones (T_{sea} at -0.5 m) measurements across an eddy near 11°S, with anti-cyclonic currents (at -5 m) shown by vectors, in Region C. Lower-left panel shows time-series of T_{sea} measurements by the different instruments. Lower-right panel shows distribution of air-sea temperature differences measured by two SWIFT buoys 4 UTC Feb 4 to 14 UTC Feb 6.

These measurements help untangle spatial from temporal variability, with both a secular (seasonal) cooling of surface waters over the course of the campaign and a variable, but at times pronounced, diel-cycle. Fig. 17. In addition, CTD casts, lower atmospheric profiling (with a mini-MPCK and a Quadcopter), and eddy-covariance measurements from an outrigger mast, were performed by the R/V Meteor as it steamed up and down the −57.25°E meridian bisecting the EUREC^{4}A-Circle just upwind of Caravela's box. Rounding out the measurements in this region were low-level Twin-Otter, ATR (as part of its 'L' pattern) legs, and BOREAL UAS measurements, as well as airborne remote sensing of sea-surface temperatures along the EUREC^{4}A-Circle by HALO.

The effect of ocean sub-mesoscale processes on air-sea interactions were the focus of measurements in Region B (Fig. 1). On two occasions the R/V Ron Brown deployed six SWIFT drifters (spar buoys) in regions of surface heterogeneity; once in January near the NTAS buoy, and again in early February near 55°W. The deployments were performed coordinated with further measurements by the R/V Ron Brown, as well as by the P3, two wave-gliders and a saildrone. The P3 (see also Fig. 4 and Fig. 2) dropped AXBTs around the SWIFTS, quantified air-sea exchange with near surface flight legs, and surveyed the near surface wind and wave fields using remote sensing. Fig. 17 documents how, during the February deployment, the SWIFTS sampled large 0.5 K mesoscale (ca 30 km) variability in SST features. This variability give rise to air-sea temperature differences twice as large as the baseline, as inferred from the average of measurements over longer periods (i.e., as shown by the Saildrone data (orange lines) and is characteristic of the SWIFT data away from the local feature in surface temperatures (e.g., green-solid line in Fig. 17). The small (0.45 K)

In the Boulevard des Tourbillons (Region C) coordinated sampling between Saildrones and two research vessels aimed to quantify the role of air-sea interaction on ocean eddies. Strong near-surface currents, with a circulation indicative of an NBC ring, were measured by the Saildrones (Fig. 17). These measurements were coordinated with the activities of the R/V Atalante and R/V MS-Merian, and three sea-gliders (e.g., Fig. 4). Extensive vertical profiling, also by high-speed underway CTDs, aimed to quantify the effect of large-mesoscale eddies on surface exchange processes, and vice versa. Being able to resolve the thermal structure of the upper ocean, should also help quantify the importance of the $O(0.3\,\mathrm{K})$ cool-skin effect and diurnal warming just below the skin-layer (Fairall et al., 1996) on ocean mixing and air-sea exchange.

Figure 18. Place holder for figure showing CO2 and ocean biology measurements.

Although EUREC^{4}A focused on the physical systems, measurements of pCO_2 were made on the R/V Atalante, R/V MS-Merian and the R/V Ron Brown (Fig. 18. In addition, both the R/V MS-Merian and R/V Meteor regularly sampled water at four different depths (selected

based on chlorophyll concentrations) for N_2 fixation and primary production rate incubations. DNA- and RNA-based sequencing will additionally be performed on these water samples, as will immunolabelling to identify diazotrophic community members, potentially including so far unrecognized members. Furthermore, large floating mats of seaweed of the genus Sargassum were observed from all crewed platforms. On the R/V MS-Merian, to investigate if, and to what degree, this biomass contributes to local N_2 fixation, primary production and methane production, incubation experiments including stable isotopes were conducted on sea-grass samples that were collected underway. In addition to extending studies of air-sea interaction to incorporate chemical and biological processes, EUREC^{4}A may also shed light on the role of meso and submeso-scale ocean circulations on these chemical and biological processes.

3.6 Benchmarks for modelling and satellite retrievals

The range of scales and types of processes that can presently be captured by both satellites and models, and the extent to which they were integrated into EUREC^{4}A's experimental design (cf., Bony et al., 2017), allows EUREC^{4}A to address questions that could not be addressed with data from earlier field studies. For instance, what resolution is required for atmospheric models with an explicit (fluid-dynamical) representation of clouds and convection to represent the vertical structure of the lower troposphere, and its interaction with mesoscale vertical motion and upper ocean variability, within the observational uncertainty? The fine-scale of the EUREC^{4}A measurements also makes it possible to quantify satellite retrieval uncertainty, for instance for measurements of small scale precipitation features, cloud microphysical properties, or column energy budgets (Illingworth et al., 2015).

For these purposes EUREC^{4}A was closely coordinated with efforts to develop and test a new generation of Earth-system models. Recently, following the pioneering efforts of Japanese colleagues (Tomita et al., 2005), a number of groups in other countries have demonstrated – within the DYAMOND[3] project (Stevens, Satoh, et al., 2019) – the capability of performing km-scale simulations on global grids (Satoh et al., 2019). A follow up, called DYAMOND-Winter is extending this capability to also include coupled global models and has been coordinated to simulate the EUREC^{4}A period. DYAMOND-Winter simulations (Klocke et al., in preparation) are being initialized from observational analyses on 20 Jan, and run for at least forty-days. With grid-scales of a few km the simulations explicitly represent scales of motion similar to those observed, all as part of a consistently represented global circulation. This enables investigations of processes influencing the mesoscale organization of fields of shallow convection, including the possible role of surface ocean features, as well as a critical evaluation of the simulations.

An example of a DYAMOND-Winter simulation using ICON is given in Fig. 19. The simulated cloud fields exhibit rich mesoscale variability whose structure, while plausible, begs a more quantitative evaluation. The combination of the field measurements and simulations with realistic variability on the mesoscale, will aid efforts to test retrievals of physical quantities from satellite radiances. This should make it possible to establish a self consistent and quantitative understanding of controls on cloudiness.

In addition to the global coupled modelling activities EUREC^{4}A is coordinating modelling activities using much higher resolution (meters to tens of meters) simulations of the ocean and atmosphere over a limited area. These will include idealized simulations with doubly periodic boundary conditions, atmospheric simulations designed to track the Lagrangian evolution of the flow, and simulations with open boundaries matched either to meteorological analyses or the free running global simulations. Few if any field studies have benefited from such a rich complement of modelling activities.

[3] the DYnamics of the Atmospheric general circulation Modeled On Non-hydrostatic Domains

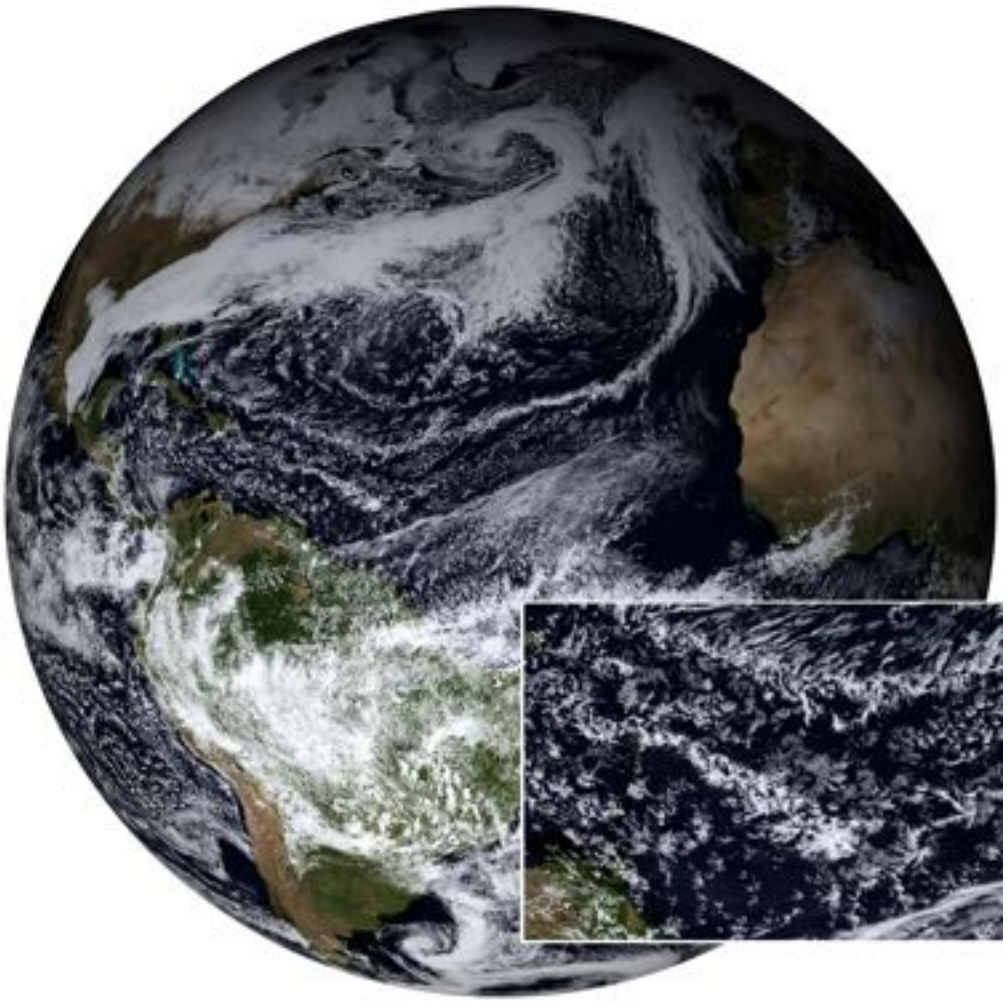

Figure 19. Global 2.5 km mesh coupled simulations performed by ICON as part of DYAMOND-Winter for the EUREC^{4}A period. The snapshot, with a zoom over the study region to show the degree of detail in the simulations, was taken from Feb 2 of a simulation initialized on January 20 and allowed to freely evolve thereafter.

Some of the challenges to evaluating these simulations are illustrated with the help of preliminary, but idealized, large-eddy simulations with the forcing specified based on preliminary data in a manner similar to what has been adopted in past studies (e.g., Stevens et al., 2005; vanZanten et al., 2011), albeit over considerably larger domains. Fig. 20 shows, with the help of a satellite image, the degree of mesoscale cloud variability. This apparent whimsicality suggests that, given the imprecision in the forcing and the cloud retrievals, assessing the magnitude of systematic biases in the simulations will be a challenge. In this case, the simulations, performed for the mean conditions in the vicinity of 'D', seems implausible, the challenge will be to assess to what extent this reflects imprecision in the forcing, of the sort that differentiates the different marked regions in the figure.

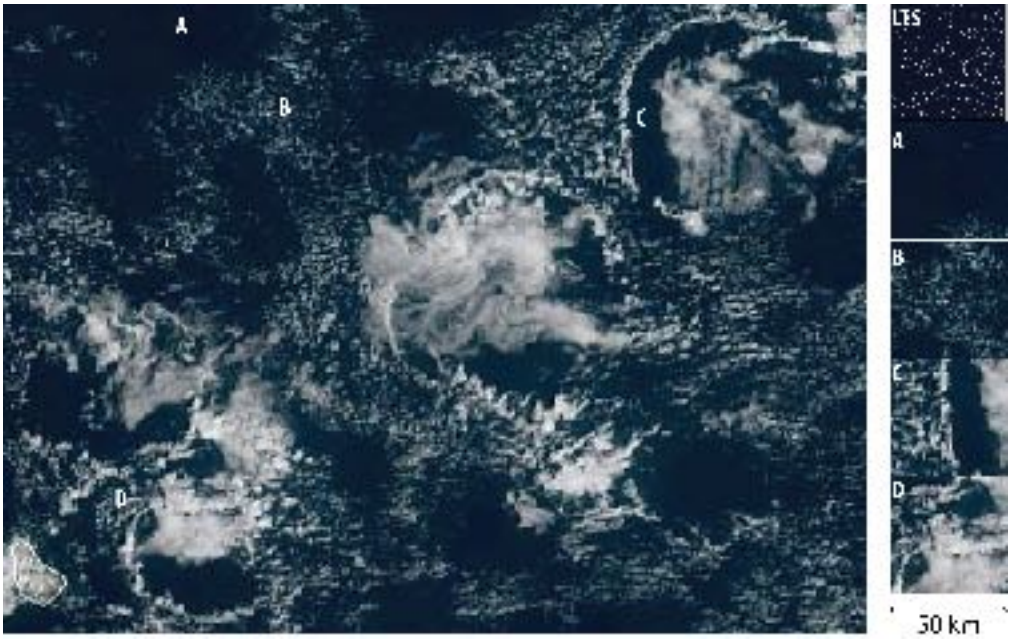

Figure 20. Geostationary satellite image showing the cloud field in the measurement area on 5 February, 2020. Snapshots of cloud fields over 50 km×50 km subdomains labeled 'A' to 'D' are compared to large-eddy simulation. The Large-eddy simulation employed a 100 m mesh and was configured in the traditional way with doubly periodic horizontal boundary conditions and with an applied horizontally homogeneous mean forcing estimated from measurements in the vicinity of subdomain 'D'.

Given a demonstration that fine-scale models can quantitatively represent the macro-structure of the observed clouds, EUREC^{4}A measurements are expected to provide benchmarks for the simulation of cloud microphysical process. This would allow the first ever evaluation of the ability of microphysical models, which depend on a variety of parameterized processes, to quantitatively represent precipitation formation processes in realistically simulated cloud fields. Previous attempts (Ackerman et al., 2009; vanZanten et al., 2011) at making such an evaluation have highlighted large differences in models, but it remains unclear to what extent these differences are due to the representation of cloud macrophysics, versus microphysics. Greater confidence in the fidelity of these simulation approaches will also greatly benefit their application to questions in remote sensing.

3.7 Scientific outreach and capacity building

Beyond the breadth of research activities that took place, EUREC^{4}A also encouraged a rich human and scientific experience through interactions with Barbadians, the regional research

community, and within the larger community of scientists from outside of the region. Activities that permitted these exchanges included operational support for flight planning, weekly seminars, a larger symposium, as well as scientific outreach to schools and to the general public. The ability to share expertise and facilities and form bonds around a common purpose, namely to better understand clouds in the trades, became an integral part of the campaign.

3.7.1 Operational support

Operational meetings took place each morning at the Regional Security Service for daily reports and coordination of the different platforms. Because of the few day predictability of weather processes, the overall coordination had to be adjusted on a daily basis, and scientists from regional weather services supported the effort with daily weather forecasts in order to coordinate the measurements for the following days. These operational meetings were also an opportunity for scientists from different teams to discuss and analyze the first results of the campaign and the perspectives ahead. Here it was learned that the mesoscale cloud pattern identified as 'Fish' in the recent literature, have long been known in the regional forecast community as *Rope clouds*.

3.7.2 Symposium and scientific seminars

Rich encounters were enabled by the organization of numerous scientific presentations. Weekly seminars provided an opportunity for exchange among EUREC^{4}A participants and local researchers at CIMH, to help facilitate collaborations extending well beyond the campaign itself. Keynote presentations at the Barbados Museum and Historical Society brought to a general audience the questions of the EUREC^{4}A campaign, as well as those surrounding the history of Caribbean hurricanes and their potential for change in a warmer climate. Campaign participants also celebrated the 50th anniversary of the BOMEX field campaign with a two-day public symposium entitled *From BOMEX to EUREC^{4}A*. It brought together a wide audience, including regional and international scientists, EUREC^{4}A participants, and students from local universities. The symposium was a tribute to a landmark campaign in meteorological and oceanographic research – the Barbados Oceanographic and Meteorological EXperiment (BOMEX) – providing an opportunity to reflect upon the evolution of climate research during the past half-century. From fascinating speeches by BOMEX veterans, to presentations describing the state of present day understanding as expressed in EUREC^{4}A's objectives, the symposium helped contextualize the efforts being made as part of EUREC^{4}A.

3.7.3 Scientific outreach in schools and facility visits

Scientific outreach in schools and facility visits sought to reinforce local environmental initiatives and highlight Barbados' unique positioning for the study of the climate and climate change. Together with the Caribbean Institute for Meteorology and Hydrology, and the Barbados Ministry of Education, ten visits to primary and secondary schools in Barbados were arranged. Simple experiments were deigned and performed with the children to help build intuition as to the underlying atmospheric and ocean processes relevant to EUREC^{4}A's scientific objectives, not to mention the weather phenomena that surrounds them on a daily basis.

Outreach activities also took the form of open houses, including guided tours of many of the measurement platforms. This included tours of the ships, visits to the BCO at Deebles point (where visitors could help launch radiosondes, the aerosol measurement facility on nearby Ragged Point, BOREAL and CU-RAAVEN drone launches at Morgan Lewis, and the POLDIRAD radar in St Johns. As an informal complement to the symposium, the outreach activities provided a window into daily life of the campaign and gathered a diverse audience, from Barbados inhabitants to the scientists involved in EUREC^{4}A. The success of EUREC^{4}A's outreach efforts are perhaps best exemplified by the ad hoc team of young engineers (Fig 22) that helped flight proof the drones before their launch from Morgan Lewis beach.

Figure 21. Group photo showing participants in the symposium "From BOMEX to EUREC^{4}A" (Photo by F. Batier).

Other initiatives included a contribution to the Barbadian project to plant one million trees before the end of the year with a handful of tree planting activities. In parallel to the scientific campaign, two French filmmakers also stayed on Barbados for the duration of EUREC^{4}A to shoot a documentary combining scientific, cultural and historical elements of the island of Barbados, from their material an additional short scientific documentary of the campaign was also created. It is provided as an electronic supplement to this manuscript.

4 Scientific Practice

EUREC^{4}A strove to advance a culture of open and collaborative use of data. It did so by initiating a series of discussions, starting well before the field campaign and culminating in a document outlining principles of good scientific practice. In arriving at these principles emphasis was placed on understanding the differing cultural contexts in which data is collected. For instance, the degree to which measurements are made by individual investigators, or made for investigators by institutions, were often colored by different national practice. Differences in how measurements are made drive differences in expectations as to how the resultant should be made available and used, and thus reflect this national coloring. EUREC^{4}A defined 'Good Scientific Practice' in terms of four principles, summarized below:

1. To actively support the initial dispersal of data by making (even preliminary) data available to *everyone* as quickly as possible through the AERIS archive.
2. To publish finalized data in ways that ensure open and long-term availability and bestow appropriate credit on those who collected it.
3. To actively attempt to meaningfully involve those who collected data in its analysis at the early stages of its use.
4. To provide clear timely and unprompted feedback on the use of the data, both by the analysis community for the instrument groups and vice versa.

Figure 22. Local children helping to evaluate air-worthiness of CU-RAAVEN UAS prior to launch from Morgan Lewis Beach (Photo By S. Bony).

In addition, examples of 'bad practice' were outlined. For example, using someone's data to write a paper and then sending the paper to the data-providers as it is about to be submitted and offering authorship was deemed bad practice. 'Good practice' would have been to intellectually involve the data provider at an early stage of the study. 'Good practice' also recognized the importance of providing intellectual space for young scientists to independently develop their ideas, and have the time to appreciate and savour the low hanging fruit to be found along their path of research.

Whereas co-authorship on the basis of status rather than through substantive contributions was generally defined as 'Bad practice' For authorship of this overview paper a very broad brush was adopted, as it was deemed desirable to recognize all technical/scientific contributions in at least one place. In this regard the ways in which each author contributed to EUREC^{4}A are summarized in an electronic supplement to this paper.

4.1 Data

The data collected during EUREC^{4}A will, in different stages of development, be uploaded and archived on the AERIS datacenter. AERIS datacenter is part of the French Data Terra Research Infrastructure, it has the objective to facilitate and enhance the use of atmospheric data, whether from satellite, aircraft, balloon, or ground observations, or from laboratory experiments. It generates advanced products and provides services to facilitate data use, to prepare campaigns, and to interface with modelling activities.

In addition, emphasis is being placed on the publishing of datasets through a special collection of articles in *Earth System Science Data*. Many of these data papers will involve the construction of cross-platform datasets, for instance for the upper-air network, or dropsondes, isotope measurements, or classes of remote sensors. At the end of the data collection phase, all data on AERIS will be mirrored by the Caribbean Institute for Meteorology and Hydrology in Barbados.

4.2 Ecology

EUREC^{4}A was largely motivated by an interest to better anticipate how Earth's climate will change with warming. This makes it all the more relevant to ask to what extent EUREC^{4}A actually exacerbates the problems it attempts to understand, or more generally whether it made appropriate use of scarce resources. The first step in answering this question is to estimate the magnitude of its environmental impact, which we do here mostly in terms of its carbon footprint. The overwhelming impact was in the use of fossil fuels (kerosene and diesel) to power the research platforms. We estimated 1.5 Gg of CO_2 emissions from aircraft operations, and about twice these emissions from ship operations. The carbon footprint associated with the travel of the participating scientists was estimated to be about a third of the emissions from the research aircraft.

A minor factor, albeit the one that is most often raised as a cause for concern is the pollution associated with the many radio and dropsondes that were launched. We calculated that batteries in the roughly 1200 sondes dropped by HALO and the P3 resulted in 1.2 kg of lithium being deposited within the ocean. Considering that seawater is the largest source of lithium, with similar amounts found in just the sea-water displaced by one research vessel, this impact appears minor. An additional source of pollution is the plastic sensor casings, but this impact is likely negligible compared to the impact of bringing the sondes by aircraft to their launch point. On the other hand, the use of such small measurement devices, and particularly the intensive use of autonomous vehicles, opens the door to better and less energy intensive way of sampling the environment.

Some validation for the use of the resources was experienced through the course of the campaign itself. This, as discussed in § 3.7, arose from the bonds that were established and the many opportunities that were presented through the numerous outreach and capacity building activities (Fig. 22). Further validation of campaign's use of resources depends ultimately on what is done with the data. That is something where we, the scientific community, has considerable influence. We very much hope it motivate a determination to learn as much as possible from the measurements that were made, also through support of funding agencies; as well as a commitment to sharing what was learned as widely and freely as possible.

5 Conclusions

Field studies are common and ongoing, and each, if only by virtue of taking a snapshot of nature at a given point in time and space, is unique and unprecedented. Field studies involving such a large number of investigators and such a large degree of coordination as was the case in EUREC^{4}A are less common, but this in itself does not represent anything more than an organizational achievement. Many of the questions EUREC^{4}A attempted to address have been the focus of past field studies. For instance, air-sea interaction was at the heart of the original Barbados field study, BOMEX (Holland & Rasmusson, 1973). Likewise a great number of studies, most recently the Convective Precipitation Experiment (Leon et al., 2016) and Rain in Cumulus over the Ocean (RICO Rauber et al., 2007), had warm rain formation processes as a central focus. The influence of boundary layer processes on cloud formation was already extensively studied by Malkus (1958), and again more recently by Albrecht et al. (2019). Field studies to measure aerosol-cloud interactions are myriad and include very large international efforts such as the Indian Ocean Experiment (Ramanathan et al., 2001). And with new insights from modelling, an increasing number of studies have begun to focus on ocean meso and submesoscale dynamics (Shcherbina et al., 2013; Buckingham et al., 2016; D'Asaro et al., 2018). What made EUREC^{4}A an advance was that in its attempt to quantify a single process, namely the link between circulation and cloudiness. This opened the door to characterizing the totality of processes believed to influence the structure of the lower atmosphere and upper ocean in the region of the trades.

At this time we can report that the execution of EUREC^{4}A was successful. All of the measurements we set out to make have been made. In retrospect, with the worldwide spread of the COVID-19 Pandemic shortly after field operations concluded, this ends up being a stroke of even greater fortune. For some key measurements, such as those of the mean mesoscale vertical motion field, preliminary analyses (e.g., Fig. 9) suggest that they have the desired information content. The analysis of other measurements, such as those that aim to quantify clouds, is more delicate and ongoing. Together we anticipate that at the conclusion of this analysis we will have learned a great deal more about the ways of clouds, how they couple to circulation systems on different scales, how they influence and are influenced by the upper ocean, and the extent to which they are susceptible to perturbations in the aerosol environment. A better quantification of these sensitivities will help us understand to what extent a warmer world will express the majesty of clouds less markedly.

Appendix A Platforms

A1 Barbados Cloud Observatory (BCO)

The BCO is physically and permanently located at Deebles Point, but during EUREC^{4}A measurements from elsewhere on the island were associated with the BCO, thiese inlcude the aerosol sampling at Ragged Point, across a cove from the BCO where a long term measurement site, run by the Caribbean Institute of Meteorology and Hydrology and the University of Miami, is also located, and a few kilometers to the northwest (near St. John) where the Polidrad was installed.

Instrument	Quantity	Brief Description
CORAL-Radar	Clouds and precipitation	High-powered K-band polarized doppler cloud radar (Stevens et al., 2016)
CORAL-Lidar	Water vapor, temperature and aerosol profiling	High-powered Raman Lidar (Stevens et al., 2016)
BCO-Pro	Water vapor, condensate and temperature profiling	RPG Microwave raditometer
Ceilometer	Aerosol & cloud detection	Jen-Optik 15K ceilometer
Micro-rain Radar	Precipitation	K-band doppler precipitation radar
Wind lidar	Wind profiling	Scanning to provide horizontal winds in lower km
Laser spectrometer	water stable isotopologues	1 Hz off-axis integrated cavity output spectrometer from Los Gatos
Laser spectrometer	water stable isotopologues	0.5 Hz cavity ring-down spectrometer from Picarro
...		

A2 SAFIRE ATR

Instrument	Quantity	Brief Description
ALIAS lidar	Clouds and aerosols	Horizontally-staring backscatter lidar operating at 355 nm and detecting polarization (Chazette et al., 2020)
BASTA radar	Clouds, precipitation and wind	Horizontally-staring bistatic FMCW 95 GHz Doppler cloud radar
RASTA radar	Clouds, precipitation and wind	Upward looking 95 GHz Doppler pulsed cloud radar
Picarro isotopes	Water stable isotopologues	Cavity ring-down laser spectrometer L2130
WVSS2	Water vapor	Absolute humidity sensor (tunable diode laser absorption)
Licor-7500	Water vapor	Humidity sensor (1-2 Hz)
KH-20	Water vapor	Fast humidity sensor (10 Hz)
Camera	Clouds	High-resolution visible cameras (Prosilica GT 1930) looking sideways and downward
UHSAS	Microphysics	Particle sizes 60 nm to 1μm
FSSP 300	Microphysics	Particle sizes 0.3 to 20 μm
CDP/FCDP	Microphysics	Particle sizes 2 and 50 μm
2D-S	Microphysics	Particle sizes 10 to 2000 μm
LWC300	Clouds	Liquid water content
Pyrgeometer	Radiation	Zipp and Zonen hemispheric broadband upwelling and downwelling longwave (4.5 - 42 μm) radiative fluxes

Pyranometer	Radiation	Zipp and Zonen hemispheric broadband upwelling and downwelling shortwave (200 - 3600 nm) radiative fluxes
CLIMAT CE332	SST	Three channel downward staring measurements of infrared irradiance at 8.7, 10.8, and 12.0 μm

$ATR-42$

A3 Woods Hole NTAS-Buoy

The Northwest Tropical Atlantic Station (NTAS) is a surface mooring maintained at approximately 15° N, 51 W since 2001 by means of annual mooring “turnarounds" – deployment of a refurbished mooring and recovery of the old mooring. The refurbished mooring has freshly calibrated sensors and is deployed first. A one to two-day period of overlap before recovering the old mooring provides intercomparison data and allows consecutive data records to be merged. Meteorological variables suitable for estimation of air-sea fluxes from bulk formulas, as well as upper ocean variables and deep ocean temperature and salinity are measured. Data are available from the Upper Ocean Processes Group at http://www.uop.whoi.edu and from OceanSITES at http://www.oceansites.org/data.

Instrument	Measurement	Sample Rate	Note
ASIMET	air temperature, relative humidity, barometric pressure, precipitation, wind speed, wind direction, longwave broadband irradiance, shortwave broadband irradiance, sea-surface temperature, sea-surface salinity	1	On surface buoy, sensors at ~3 m height.
Vaisala WXT 520	air temperature, relative humidity, barometric pressure, precipitation, wind speed, wind direction		Sensor at 3 m height
Seabird SBE-39	air temperature	5	Sensor at 3 m height
Seabird SBE-56	sea-surface temperature	1	In buoy hull
Xeos Brizo	surface wave height and period	60	20 min sample interval each hour
Seabird SBE-37	Temperature and salinity	10	On mooring line at 10, 25, 40, 55 and 70 m
Seabird SBE-39	Temperature	5	On mooring line at 5, 15, 20, 30, 35, 45, 50, 60, 65, 75, 80, 90, 100 and 110 m
Star-Oddi Starmon	Temperature	10	On mooring line at 110-160 m, 10 m intervals
Nortek Aquadopp	Horizontal velocity	20	On mooring line at 5.7 and 13 m
Nortek Aquapro	Horizontal velocity profile	60	On mooring line at 24 m, uplooking
Teledyne RDI ADCP	Horizontal velocity profile	60	On mooring line at 85 m, uplooking
Seabird SBE-37	Deep ocean temperature and salinity	5	38 m above bottom

A4 Saildrones

A5 Applied Physics Lab SWIFTs and Sea-gliders

A6 Surface Drifters

Appendix B Brief summary of contributions by author

Here we intend to publish the author contributions following what was entered in the registration sheet, perhaps modified by subsequent and direct contributions to the paper. The purpose would to readers parse the large author list and understand the roles of the different authors.

Acknowledgments
The deployment of the AutoNaut Caravela and the three UEA Seagliders was supported by funding from the European Research Council (ERC) under the European Union's Horizon 2020 research and innovation programme (COMPASS, Grant agreement No. 74110).

References

Ackerman, A. S., vanZanten, M. C., Stevens, B., Savic-Jovcic, V., Bretherton, C. S., Chlond, A., … Zulauf, M. (2009). Large-Eddy Simulations of a Drizzling, Stratocumulus-Topped Marine Boundary Layer. *Mon Weather Rev*, *137*(3), 1083–1110.

Albrecht, B., Bretherton, C. S., Johnson, D., Schubert, W. S., & Frisch, A. S. (1995). The Atlantic stratocumulus transition experiment – ASTEX. *Bulletin of the American Meteorological Society*, *76*, 889–904.

Albrecht, B., Ghate, V., Mohrmann, J., Wood, R., Zuidema, P., Bretherton, C., … Schmidt, S. (2019, January). Cloud System Evolution in the Trades (CSET): Following the Evolution of Boundary Layer Cloud Systems with the NSF–NCAR GV. *Bull. Amer. Meteor. Soc.*, *100*(1), 93–121.

Augstein, E., Schmidt, H., & Ostapoff, F. (1974, March). The vertical structure of the atmospheric planetary boundary layer in undisturbed trade winds over the Atlantic Ocean. *Boundary-Layer Meteorol*, *6*(1-2), 129–150.

Bailey, A., Toohey, D., & Noone, D. (2013, August). Characterizing moisture exchange between the Hawaiian convective boundary layer and free troposphere using stable isotopes in water. *Journal of Geophysical Research: Atmospheres*, *118*(15), 8208–8221.

Bannon, J. K. (1949). Large-scale vertical motion in the atmosphere. *Nature*, *163*, 495–496.

Bodenschatz, E., Malinowski, S. P., Shaw, R. A., & Stratmann, F. (2010). Can we understand clouds without turbulence? *Science*, *327*, 970–971.

Bony, S., Schulz, H., Vial, J., & Stevens, B. (2020, January). Sugar, Gravel, Fish and Flowers: Dependence of Mesoscale Patterns of Trade-wind Clouds on Environmental Conditions. *Geophys. Res. Lett.*, *47*(7), 2019GL085988–9.

Bony, S., & Stevens, B. (2019, March). Measuring Area-Averaged Vertical Motions with Dropsondes. *J. Atmos. Sci*, *76*(3), 767–783.

Bony, S., Stevens, B., Ament, F., Bigorre, S., Chazette, P., Crewell, S., … Wirth, M. (2017, September). EUREC4A: A field campaign to Elucidate the Couplings between Clouds, Convection and Circulation. *Surv Geophys*, *36*(1), 1529–1568.

Bony, S., Stevens, B., Frierson, D. M. W., Jakob, C., Kageyama, M., Pincus, R., … Webb, M. J. (2015, March). Clouds, circulation and climate sensitivity. *Nature Geoscience*, *8*(4), 261–268.

Bretherton, C. S., Krueger, S. K., Wyant, M. C., Bechtold, P., van Meijgaard, E., Stevens, B., & Teixeira, J. (1999). A GCSS Boundary-Layer Cloud Model Intercomparison Study Of The First Astex Lagrangian Experiment. *Boundary-Layer Meteorol*, *93*(3), 341–380.

Brient, F., Schneider, T., Tan, Z., Bony, S., Qu, X., & Hall, A. (2016). Shallowness of tropical low clouds as a predictor of climate models' response to warming. *Climate Dynamics*,

47(1-2), 433–449.

Broadwell, J. E., & Breidenthal, R. E. (1982, January). A simple model of mixing and chemical reaction in a turbulent shear layer. *Journal of Fluid Mechanics*, *125*, 397–410.

Brummer, B., AUGSTEIN, E., & Riehl, H. (1974, January). On the low-level wind structure in the Atlantic trade. *Q.J.R. Meteorol. Soc.*, *100*(423), 109–121.

Buckingham, C. E., Garabato, A. C. N., Thompson, A. F., Brannigan, L., Lazar, A., Marshall, D. P., … Belcher, S. E. (2016). Seasonality of submesoscale flows in the ocean surface boundary layer. *Geophys. Res. Lett.*, *43*(5), 2118–2126.

Callies, J., & Ferrari, R. (2013, November). Interpreting Energy and Tracer Spectra of Upper-Ocean Turbulence in the Submesoscale Range (1–200 km). *J. Phys. Oceanogr.*, *43*(11), 2456–2474.

Carton, X. (2010, March). Oceanic Vortices. In *Fronts, waves and vortices in geophysical flows* (pp. 61–108). Berlin, Heidelberg: Springer Berlin Heidelberg.

Chazette, P., Totems, J., Baron, A., Flamant, C., & Bony, S. (2020). Trade-wind clouds and aerosols characterized by airborne horizontal lidar measurements during the EUREC⁴A field campaign. *Earth System Science Data Discussions*, 1–2.

Chelton, D. B., & Xie, S.-P. (2010, December). Coupled Ocean-Atmosphere Interaction at Oceanic Mesoscales. *Oceanography*, *23*(4), 52–69.

Cooper, W. A., Lasher-Trapp, S. G., & Blyth, A. M. (2013, July). The influence of entrainment and mixing on the initial formation of rain in a warm cumulus cloud. *Journal of the Atmospheric Sciences*, *70*(6), 1727–1743.

D'Asaro, E. A., Shcherbina, A. Y., Klymak, J. M., Molemaker, J., Novelli, G., Guigand, C. M., … Özgökmen, T. M. (2018, February). Ocean convergence and the dispersion of flotsam. *Proc Natl Acad Sci USA*, *115*(6), 1162–1167.

Denby, L. (2020, January). Discovering the Importance of Mesoscale Cloud Organization Through Unsupervised Classification. *Geophys. Res. Lett.*, *47*(1), 1097–10.

Dixit, V. V., Nuijens, L., & Helfer, K. C. (2020). Counter-gradient momentum transport through subtropical shallow convection in ICON-LEM simulations. *Earth and Space Science Open Archive*, 23.

Fairall, C. W., Bradley, E. F., Godfrey, J. S., Wick, G. A., Edson, J. B., & Young, G. S. (1996). Cool-skin and warm-layer effects on sea surface temperature. *Journal of Geophysical Research: Oceans*, *101*(C1), 1295–1308.

Foussard, A., Lapeyre, G., & Plougonven, R. (2019, June). Response of Surface Wind Divergence to Mesoscale SST Anomalies under Different Wind Conditions. *J. Atmos. Sci*, *76*(7), 2065–2082.

Garstang, M., & Betts, A. K. (1974). A Review of the Tropical Boundary Layer and Cumulus Convection: Structure, Parameterization, and Modeling. *Bulletin of the American Meteorological Society*, *55*(10), 1195–1205.

Gibson, E. R., Gierlus, K. M., Hudson, P. K., & Grassian, V. H. (2007). Generation of Internally Mixed Insoluble and Soluble Aerosol Particles to Investigate the Impact of Atmospheric Aging and Heterogeneous Processing on the CCN Activity of Mineral Dust Aerosol. *Aerosol Sci. Tech.*, *41*(10), 914–924.

Holland, J. Z., & Rasmusson, E. M. (1973). Measurements of the atmospheric mass, energy, and momentum budgets over a 500-kilometer square of tropical ocean. *Mon Weather Rev*, *101*(1), 44–55.

Illingworth, A. J., Barker, H. W., Beljaars, A., Ceccaldi, M., Chepfer, H., Clerbaux, N., … van Zadelhoff, G. J. (2015, August). The EarthCARE Satellite: The next step forward in global measurements of clouds, aerosols, precipitation, and radiation. *Bull. Amer. Meteorol. Soc*, *96*(8), 1311–1332.

Jensen, J. B., & Nugent, A. D. (2017, January). Condensational growth of drops formed on giant sea-salt aerosol particles. *Journal of the Atmospheric Sciences*, *74*(3), 679–697.

Lambaerts, J., Lapeyre, G., Plougonven, R., & Klein, P. (2013, September). Atmospheric response to sea surface temperature mesoscale structures. *Journal of Geophysical Research:*

Atmospheres, *118*.

Lapeyre, G. (2017, March). Surface Quasi-Geostrophy. *Fluids*, *2*(1), 7–28.

Laxenaire, R., Speich, S., Blanke, B., Chaigneau, A., Pegliasco, C., & Stegner, A. (2018, November). Anticyclonic Eddies Connecting the Western Boundaries of Indian and Atlantic Oceans. *Journal of Geophysical Research: Oceans*, *123*(11), 7651–7677.

Leon, D. C., French, J. R., Lasher-Trapp, S., Blyth, A. M., Abel, S. J., Ballard, S., … Young, G. (2016, July). The Convective Precipitation Experiment (COPE): Investigating the Origins of Heavy Precipitation in the Southwestern United Kingdom. *Bull. Amer. Meteor. Soc.*, *97*(6), 1003–1020.

Levin, Z., Ganor, E., & Gladstein, V. (1996, January). The effects of desert particles coated with sulfate on rain formation in the eastern Mediterranean. *J. Of Appl. Meteorol.*, *35*(9), 1511–1523.

Li, X.-Y., Brandenburg, A., Svensson, G., Haugen, N. E. L., Mehlig, B., & Rogachevskii, I. (2018, January). Effect of turbulence on collisional growth of cloud droplets. *Journal of the Atmospheric Sciences*, *75*(10), 3469–3487.

Mahadevan, A. (2016, January). The Impact of Submesoscale Physics on Primary Productivity of Plankton. *Annu. Rev. Marine. Sci.*, *8*(1), 161–184.

Malkus, J. S. (1958). *On the structure of the trade wind moist layer*. Cambridge, MA: Massachusetts Institute of Technology and Woods Hole Oceanographic Institution.

McWilliams, J. C. (2016, May). Submesoscale currents in the ocean. *Proc. R. Soc. A*, *472*(2189), 20160117–32.

Mieslinger, T., Horváth, Á., Buehler, S. A., & Sakradzija, M. (2019, November). The Dependence of Shallow Cumulus Macrophysical Properties on Large-Scale Meteorology as Observed in ASTER Imagery. *J Geophys Res-Atmos*, *124*(21), 11477–11505.

Naumann, A. K., Stevens, B., & Hohenegger, C. (2019, May). A Moist Conceptual Model for the Boundary Layer Structure and Radiatively Driven Shallow Circulations in the Trades. *J. Atmos. Sci*, *76*(5), 1289–1306.

Nencioli, F., Dong, C., Dickey, T., Washburn, L., & McWilliams, J. C. (2010, March). A Vector Geometry–Based Eddy Detection Algorithm and Its Application to a High-Resolution Numerical Model Product and High-Frequency Radar Surface Velocities in the Southern California Bight. *J. Atmos. Oceanic Technol.*, *27*(3), 564–579.

Nuijens, L., Serikov, I., Hirsch, L., Lonitz, K., & Stevens, B. (2014, February). The distribution and variability of low-level cloud in the North Atlantic trades. *Q.J.R. Meteorol. Soc.*, *140*(684), 2364–2374.

O'Neill, L. W., Chelton, D. B., & Esbensen, S. K. (2012, October). Covariability of Surface Wind and Stress Responses to Sea Surface Temperature Fronts. *Journal of Climate*, *25*(17), 5916–5942.

Prospero, J. M. (1999, March). Long-range transport of mineral dust in the global atmosphere: Impact of African dust on the environment of the southeastern United States. *Proc Natl Acad Sci USA*, *96*(7), 3396–3403.

Pujol, M.-I., Faugère, Y., Taburet, G., Dupuy, S., Pelloquin, C., Ablain, M., & Picot, N. (2016). DUACS DT2014: the new multi-mission altimeter data set reprocessed over 20 years. *Ocean Sci.*, *12*(5), 1067–1090.

Ramanathan, V., Crutzen, P. J., Lelieveld, J., Mitra, A. P., Althausen, D., Anderson, J., … Valero, F. P. J. (2001). Indian Ocean Experiment: An integrated analysis of the climate forcing and effects of the great Indo-Asian haze. *Journal of Geophysical Research: Atmospheres*, *106*(D22), 28371–28398.

Rasp, S., Schulz, H., Bony, S., & Stevens, B. (2020). Combining crowd-sourcing and deep learning to understand meso-scale organization of shallow convection . *Bulletin of the American Meteorological Society*, in review.

Rauber, R. M., Stevens, B., Ochs III, H. T., & Knight, C. (2007). *Rain in shallow cumulus over the ocean–The RICO campaign, B. Am. Meteorol. Soc., 88, 191 2, doi: 10.1175.*

Renault, L., McWilliams, J. C., & Gula, J. (2018, September). Dampening of Submesoscale Currents by Air-Sea Stress Coupling in the Californian Upwelling System. *Sci Rep*, *8*(1),

1–8.

Renault, L., Molemaker, M. J., McWilliams, J. C., Shchepetkin, A. F., Lemarie, F., Chelton, D., … Hall, A. (2016, June). Modulation of Wind Work by Oceanic Current Interaction with the Atmosphere. *J. Phys. Oceanogr.*, *46*(6), 1685–1704.

Rieck, M., Nuijens, L., & Stevens, B. (2012). Marine boundary layer cloud feedbacks in a constant relative humidity atmosphere. *J. Atmos. Sci*, *69*(8), 2538–2550.

Riehl, H., YEH, T. C., Malkus, J. S., & LASEUR, N. E. (1951). The North-East Trade of the Pacific Ocean. *Q.J.R. Meteorol. Soc.*, *77*(334), 598–626.

Rocha, C. B., Chereskin, T. K., Gille, S. T., & Menemenlis, D. (2016, February). Mesoscale to Submesoscale Wavenumber Spectra in Drake Passage. *J. Phys. Oceanogr.*, *46*(2), 601–620.

Satoh, M., Stevens, B., Judt, F., Khairoutdinov, M., Lin, S.-J., Putman, W. M., & Düben, P. (2019, May). Global Cloud-Resolving Models. *Curr Clim Change Rep*, *5*(3), 172–184.

Seifert, A., & Heus, T. (2013). Large-eddy simulation of organized precipitating trade wind cumulus clouds. *Atmos. Chem. Phys.*, *13*(11), 5631–5645.

Shcherbina, A. Y., D'Asaro, E. A., Lee, C. M., Klymak, J. M., Molemaker, M. J., & McWilliams, J. C. (2013, September). Statistics of vertical vorticity, divergence, and strain in a developed submesoscale turbulence field. *Geophys. Res. Lett.*, *40*(17), 4706–4711.

Sherwood, S. C., Bony, S., & Dufresne, J.-L. (2014, January). Spread in model climate sensitivity traced to atmospheric convective mixing. *Nature*, *505*(7481), 37–42.

Siebesma, A. P., Bony, S., Jakob, C., & Stevens, B. (2020). *Clouds and Climate: Climate Science's Greatest Challenge*. Cambridge, UK: Cambridge University Press.

Siebesma, A. P., Bretherton, C. S., Brown, A., Chlond, A., Cuxart, J., Duynkerke, P. G., … Stevens, D. E. (2003, May). A Large Eddy Simulation Intercomparison Study of Shallow Cumulus Convection. *J. Atmos. Sci*, *60*(1), 1201–1219.

Snodgrass, E. R., Di Girolamo, L., & Rauber, R. M. (2009, March). Precipitation Characteristics of Trade Wind Clouds during RICO Derived from Radar, Satellite, and Aircraft Measurements. *J. Of Appl. Meteorol.*, *48*(3), 464–483.

Stephan, C. C., Schnitt, S., Schulz, H., Bellenger, H., de Szoeke, S. P., Acquistapace, C., … Stevens, B. (2020, August). Ship- and island-based atmospheric soundings from the 2020 EUREC⁴A field campaign. *Earth System Science Data Discussions*, 1–35.

Stevens, B., Ackerman, A. S., & Albrecht, B. A. (2001). Simulations of Trade Wind Cumuli under a Strong Inversion . *Journal of the Atmospheric Sciences*, *58*(14), 1870–1891.

Stevens, B., Ament, F., Bony, S., Crewell, S., Ewald, F., Gross, S., … Zinner, T. (2019, June). A High-Altitude Long-Range Aircraft Configured as a Cloud Observatory: The NARVAL Expeditions. *Bull. Amer. Meteor. Soc.*, *100*(6), 1061–1077.

Stevens, B., Bony, S., Brogniez, H., Hentgen, L., Hohenegger, C., Kiemle, C., … Zuidema, P. (2019, November). Sugar, gravel, fish and flowers: Mesoscale cloud patterns in the trade winds. *Q.J.R. Meteorol. Soc.*, *146*(726), 141–152.

Stevens, B., Farrell, D., Hirsch, L., Jansen, F., Nuijens, L., Serikov, I., … Prospero, J. M. (2016, May). The Barbados Cloud Observatory: anchoring investigations of clouds and circulation on the edge of the ITCZ. *Bull. Amer. Meteorol. Soc*, *97*(5), 787–801.

Stevens, B., Lenschow, D. H., & Faloona, I. (2003). On entrainment rates in nocturnal marine stratocumulus. *Quarterly Journal of the Royal Meteorological Society*, *129*(595), 3469–3493.

Stevens, B., Moeng, C.-H., Ackerman, A. S., Bretherton, C. S., Chlond, A., de Roode, S., … Zhu, P. (2005). Evaluation of Large-Eddy Simulations via Observations of Nocturnal Marine Stratocumulus. *Mon Weather Rev*, *133*(6), 1443–1462.

Stevens, B., Satoh, M., Auger, L., Biercamp, J., Bretherton, C. S., Chen, X., … Zhou, L. (2019, September). DYAMOND: the DYnamics of the Atmospheric general circulation Modeled On Non-hydrostatic Domains. *Prog. in Earth and Planet. Sci.*, *6*(1), 1–17.

Stevens, B., & Schwartz, S. E. (2012, May). Observing and Modeling Earth's Energy Flows.

Surv Geophys, *33*(3-4), 779–816.

Sullivan, P. P., McWilliams, J. C., Weil, J. C., Patton, E. G., & Fernando, H. J. S. (2020). Marine boundary layers above heterogeneous SST: Across-front winds . *Journal of the Atmospheric Sciences*, 1–75– in press.

Tomita, H., Miura, H., Iga, S., Nasuno, T., & Satoh, M. (2005). A global cloud-resolving simulation: Preliminary results from an aqua planet experiment. *Geophys. Res. Lett.*, *32*(8), 3283.

vanZanten, M. C., Stevens, B., Nuijens, L., Siebesma, A. P., Ackerman, A. S., Burnet, F., … Wyszogrodzki, A. (2011, February). Controls on precipitation and cloudiness in simulations of trade-wind cumulus as observed during RICO. *Journal of Advances in Modeling Earth Systems*, *3*(2), n/a–n/a.

Vial, J., Bony, S., Dufresne, J.-L., & Roehrig, R. (2016, December). Coupling between lower-tropospheric convective mixing and low-level clouds: Physical mechanisms and dependence on convection scheme. *Journal of Advances in Modeling Earth Systems*, *8*(4), 1892–1911.

Vogel, R., Bony, S., & Stevens, B. (2020, May). Estimating the Shallow Convective Mass Flux from the Subcloud-Layer Mass Budget. *J. Atmos. Sci*, *77*(5), 1559–1574.

Wyszogrodzki, A. A., Grabowski, W. W., Wang, L. P., & Ayala, O. (2013, September). Turbulent collision-coalescence in maritime shallow convection. *Atmos. Chem. Phys.*, *13*(16), 8471–8487.

Zuidema, P., Li, Z., Hill, R. J., Bariteau, L., Rilling, B., Fairall, C., … Hare, J. (2012, January). On Trade Wind Cumulus Cold Pools. *J. Atmos. Sci*, *69*(1), 258–280.